PROCEEDINGS OF THE ROYAL SOCIETY A MATHEMATICAL, PHYSICAL & ENGINEERING SCIENCES

Constitutive modelling of arteries

Gerhard A. Holzapfel and Ray W. Ogden

Proc. R. Soc. A 2010 **466**, doi: 10.1098/rspa.2010.0058 first published online 31 March 2010

PROCEEDINGS OF THE ROYAL SOCIETY A

Proc. R. Soc. A (2010) **466**, 1551–1597
doi:10.1098/rspa.2010.0058
Published online 31 March 2010

Review

Constitutive modelling of arteries

By Gerhard A. Holzapfel[1,2,*] and Ray W. Ogden[3]

[1]*Institute of Biomechanics, Center of Biomedical Engineering, Graz University of Technology, Graz, Austria*
[2]*Department of Solid Mechanics, School of Engineering Sciences, Royal Institute of Technology (KTH), Stockholm, Sweden*
[3]*Department of Mathematics, University of Glasgow, Glasgow, UK*

This review article is concerned with the mathematical modelling of the mechanical properties of the soft biological tissues that constitute the walls of arteries. Many important aspects of the mechanical behaviour of arterial tissue can be treated on the basis of elasticity theory, and the focus of the article is therefore on the constitutive modelling of the anisotropic and highly nonlinear elastic properties of the artery wall. The discussion focuses primarily on developments over the last decade based on the theory of deformation invariants, in particular invariants that in part capture structural aspects of the tissue, specifically the orientation of collagen fibres, the dispersion in the orientation, and the associated anisotropy of the material properties. The main features of the relevant theory are summarized briefly and particular forms of the elastic strain-energy function are discussed and then applied to an artery considered as a thick-walled circular cylindrical tube in order to illustrate its extension–inflation behaviour. The wide range of applications of the constitutive modelling framework to artery walls in both health and disease and to the other fibrous soft tissues is discussed in detail. Since the main modelling effort in the literature has been on the passive response of arteries, this is also the concern of the major part of this article. A section is nevertheless devoted to reviewing the limited literature within the continuum mechanics framework on the active response of artery walls, i.e. the mechanical behaviour associated with the activation of smooth muscle, a very important but also very challenging topic that requires substantial further development. A final section provides a brief summary of the current state of arterial wall mechanical modelling and points to key areas that need further modelling effort in order to improve understanding of the biomechanics and mechanobiology of arteries and other soft tissues, from the molecular, to the cellular, tissue and organ levels.

Keywords: arterial wall mechanics; fibrous biological tissues; fibre-reinforced materials; artery layers; finite elasticity

*Author for correspondence (holzapfel@tugraz.at).

One contribution to the 2010 Anniversary Series ‘A collection of reviews celebrating the Royal Society’s 350th Anniversary’.

Received 5 February 2010
Accepted 26 February 2010

1. Introduction

The mechanical behaviour of soft biological tissues has received an increasing amount of attention in the literature in the last few years, and this is particularly the case for arterial wall tissue, although the mechanics of other tissues are also widely studied. The purpose of the present review article is to highlight and summarize recent developments in the biomechanics and mechanobiology of arterial walls, with particular reference to modelling the elastic properties of the tissue based on an approach that focuses on invariants associated with the directions of collagen fibres and their dispersion. Both the passive and the active behaviour of the tissue are considered. In so doing, we have attempted to refer to the contributions of the most recent papers, essentially from the last 10 years, although inevitably there will be important contributions that we have overlooked, for which we apologize.

The content of this review is summarized as follows. In §2, we provide an overview of the kinematical background relevant to the development of constitutive laws for fibre-reinforced materials with particular reference to the invariant formulation of constitutive laws for materials with one or two families of fibres. Particular note is made of the equations governing planar biaxial deformations since biaxial tests are commonly used protocols in arterial mechanics that provide important information about the material properties. However, it is emphasized that biaxial tests alone are not sufficient to fully characterize the material properties of the anisotropic soft tissues, as fully discussed by Holzapfel & Ogden (2009*c*), and that lack of sufficient data means that some prior assumptions about the form of the constitutive law are necessary to make progress in material characterization. With this in mind, some specific forms of strain-energy function are discussed, some merits of the particular constitutive structure are emphasized and conditions for consistency with the linear theory of transversely isotropic elasticity are noted.

Combined extension and inflation of a segment of an artery (a circular cylindrical tube) provides data that are equivalent to data obtained from planar biaxial tests. The theoretical basis for evaluating such tests is summarized in a concise form and some recently obtained representative data from the Holzapfel laboratory are illustrated. Specifically, experimental data from a human internal carotid artery are shown with the emphasis on the dependence of pressure on circumferential stretch (equivalent to the internal radius) of the artery initially pre-stretched axially by various amounts in the absence of pressure. This is both for an intact artery and for its separate media–intima composite and adventitia layers and highlights the significant differences in the mechanical properties of the different layers of the artery wall.

Section 3 provides an overview of the different applications of models based on the invariant structure of constitutive laws that were developed primarily for artery walls. The main applications are to arteries, of course, but the range of applications is quite extensive. It includes modelling both healthy and diseased arteries, accounting for viscoelastic effects, as appropriate for muscular arteries, and the simulation of clinical procedures such as balloon angioplasty. Angioplasty involves the description of three-dimensional fluid–structure interaction, inelastic/plastic effects, plaque fissuring and dissection that

occur during the intervention, and balloon–stent–artery interaction with the focus on different stent designs. Further applications deal with the development of cerebral and abdominal aortic aneurysms by considering fluid–structure interactions and an intraluminal thrombus, with criteria for arterial failure and the modelling and analysis of growth and remodelling, a key area nowadays that requires both analytical and numerical (finite element) approaches. The considered constitutive framework has also been used for modelling a wide range of other soft tissues and we provide a short summary of these applications, which include veins, intestine, the cornea, the annulus fibrosus and heart tissue, *inter alia*. In the final part of §3, we also review the usage of the considered constitutive framework in the analysis of some general aspects of soft-tissue elasticity, and note that it is even used in the modelling of textile composites.

In §4 the modelling of collagenous tissues based on preferred directions of the fibres is extended to allow for dispersion of the fibre orientations, which has a significant effect on the mechanical response of the tissue. Some novel aspects relating to a dispersion parameter used in the theory are described. In particular, at the upper limit of its allowable range of values it yields a planar isotropic distribution of fibres normal to the preferred fibre direction, and the consequences of this are discussed in some detail. In a representative example, we examine the inflation of a fibre-reinforced thin-walled circular cylindrical tube. For dispersion parameters that lie within the upper range of values the resulting pressure versus circumferential stretch response is non-monotonic and increasing radius can be associated with negative pressure. It is therefore concluded that such values of the dispersion parameter are inappropriate for the modelling of soft tissues. The relevant theory is provided for both two- and three-dimensional fibre orientation distributions and applications for which the theory has been used are discussed. These include modelling of the coronary artery (bypass graft surgery, implantation of drug-eluting stents), carotid bifurcation (effect of changes in lipid pool and calcification on wall stresses and on vulnerability), abdominal aorta (aneurysm), adaptive artery growth, mitral and aortic valves and the cornea.

In §§2–4 the focus is on the passive mechanical response of arterial tissues, which has dominated the literature. Modelling of the active response associated with smooth muscle activation has received relatively little attention but its importance cannot be underestimated. For example, smooth muscle cells control changes in arteries such as the lumen diameter and the extracellular matrix turnover. We therefore provide, in §5, pointers to the background on smooth muscle activation and a short discussion of the limited modelling that has been conducted within the continuum mechanics context. This includes purely phenomenological approaches and more recent work that combines continuum theory with active response controlled by calcium concentration. In the latter context, a meaningful approach, which is discussed briefly, is to couple a strain-energy function with a chemical model that describes smooth muscle contraction.

The concluding §6 summarizes the present situation and points to the need for research to incorporate more features in the models and to improve understanding of the interaction between mechanical, biological and chemical responses.

2. The basic building blocks of a structural model

(a) Kinematics, stress and constitutive structure

In some situations the mechanical behaviour of soft biological tissues can be regarded as elastic under relatively large deformations.

Locally, the deformation is described in terms of the deformation gradient tensor, denoted $\mathbf{F}$, and the elastic material properties can be characterized in terms of a strain-energy function, here denoted Ψ, which, in general, is a function of $\mathbf{F}$. For reasons of objectivity the dependence on $\mathbf{F}$ is through the right Cauchy–Green tensor $\mathbf{C}=\mathbf{F}^{\mathrm{T}}\mathbf{F}$. Thus, $\Psi=\Psi(\mathbf{C})$ and the associated Cauchy stress tensor $\boldsymbol{\sigma}$ is given by

$$\boldsymbol{\sigma}=2J^{-1}\mathbf{F}\frac{\partial\Psi}{\partial\mathbf{C}}\mathbf{F}^{\mathrm{T}}, \tag{2.1}$$

for a material without internal mechanical constraints, where $J=\det\mathbf{F}$. For an isotropic material Ψ depends on $\mathbf{C}$ only through its three principal invariants I_1, I_2 and I_3, which are defined by

$$I_1=\mathrm{tr}\mathbf{C},\quad I_2=\tfrac{1}{2}[(\mathrm{tr}\mathbf{C})^2-\mathrm{tr}(\mathbf{C}^2)]\quad\text{and}\quad I_3=\det\mathbf{C}. \tag{2.2}$$

For further details of the basic kinematics of finite deformations see, for example, the books by Ogden (1997) and Holzapfel (2000).

Many soft tissues can be treated as incompressible materials and justification for this is provided in the studies by, for example, Carew *et al.* (1968) in relation to arteries and Vossoughi *et al.* (1980) for myocardial tissue. For an incompressible material the constraint $I_3=\det\mathbf{C}=1$ holds and as a result the Cauchy stress tensor (2.1) has to be modified in the form

$$\boldsymbol{\sigma}=-p\mathbf{I}+2\mathbf{F}\frac{\partial\Psi}{\partial\mathbf{C}}\mathbf{F}^{\mathrm{T}}, \tag{2.3}$$

where p is a Lagrange multiplier associated with the constraint and represents a contribution to the hydrostatic stress. Note that equation (2.3) applies for any incompressible elastic material without restriction on the specific material properties. For an incompressible isotropic material Ψ depends only on I_1 and I_2, and equation (2.3) expands to

$$\boldsymbol{\sigma}=-p\mathbf{I}+2\psi_1\mathbf{B}+2\psi_2(I_1\mathbf{B}-\mathbf{B}^2), \tag{2.4}$$

where $\psi_i=\partial\Psi/\partial I_i$, $i=1,2$, and $\mathbf{B}=\mathbf{F}\mathbf{F}^{\mathrm{T}}$ denotes the left Cauchy–Green tensor.

In soft tissues the collagen component endows the material with one or more preferred directions. In the case of a single family of locally aligned collagen fibres the preferred direction can be characterized by a unit vector, here denoted $\mathbf{M}$, and the material response is then transversely isotropic. This is reflected in the form of Ψ, which we now write as $\Psi(\mathbf{C},\mathbf{M})$. Moreover, if the material properties are independent of the sense of $\mathbf{M}$ then $\Psi(\mathbf{C},-\mathbf{M})=\Psi(\mathbf{C},\mathbf{M})$ and then Ψ depends on $\mathbf{M}$ only through the tensor product $\mathbf{M}\otimes\mathbf{M}$. A transversely isotropic strain-energy function $\Psi(\mathbf{C},\mathbf{M}\otimes\mathbf{M})$ can then be regarded as an isotropic function of $\mathbf{C}$

and $\mathbf{M}\otimes\mathbf{M}$. With these two tensors are associated two additional independent invariants, which typically are taken to be

$$I_4=\mathbf{M}\cdot(\mathbf{CM})\quad\text{and}\quad I_5=\mathbf{M}\cdot(\mathbf{C}^2\mathbf{M}). \tag{2.5}$$

The invariant I_4 has a direct interpretation as the square of the stretch in the direction of the fibre, but I_5 does not have a similar immediate interpretation.

Then for an incompressible material reinforced by a single family of fibres, Ψ depends on the four invariants I_1, I_2, I_4 and I_5. In this case the Cauchy stress has two extra terms associated with the anisotropic contribution and extends to the form

$$\boldsymbol{\sigma}=-p\mathbf{I}+2\psi_1\mathbf{B}+2\psi_2(I_1\mathbf{B}-\mathbf{B}^2)+2\psi_4\mathbf{m}\otimes\mathbf{m}+2\psi_5(\mathbf{m}\otimes\mathbf{Bm}+\mathbf{Bm}\otimes\mathbf{m}), \tag{2.6}$$

where $\mathbf{m}=\mathbf{FM}$ is the push forward of $\mathbf{M}$ to the deformed configuration, while $\psi_i=\partial\Psi/\partial I_i,\ i=1,2,4,5$.

An interesting alternative to I_5 as the second transversely isotropic invariant, which does have a direct interpretation, is defined by

$$I_5^*=\mathbf{M}\cdot(\mathbf{C}^*\mathbf{M}), \tag{2.7}$$

where $\mathbf{C}^*=I_3\mathbf{C}^{-1}$ ($I_3=1$ for an incompressible material). The interpretation is based on Nanson's formula $\mathbf{n}\,\mathrm{d}a=J\mathbf{F}^{-\mathrm{T}}\mathbf{N}\,\mathrm{d}A$ connecting an infinitesimal area element $\mathrm{d}A$, with unit normal $\mathbf{N}$, in the reference configuration to the corresponding area element $\mathrm{d}a$, with unit normal $\mathbf{n}$, in the deformed configuration. With $\mathbf{N}=\mathbf{M}$ the ratio $\mathrm{d}a^2/\mathrm{d}A^2$ is given by I_5^*, and hence I_5^* is a measure of changes in area normal to the fibre direction. Note that in general $\mathbf{m}=\mathbf{FM}$ does not coincide with $\mathbf{n}$ either in magnitude or in direction. If we use I_5^* instead of I_5 and write $\Psi=\Psi^*(I_1,I_2,I_4,I_5^*)$ then the Cauchy stress has the same structure as in equation (2.6), but with different, but equivalent, coefficients. Explicitly we have

$$\begin{aligned}\boldsymbol{\sigma}=&-p\mathbf{I}+2(\psi_1^*-I_4\psi_5^*)\mathbf{B}+2(\psi_2^*+\psi_5^*)(I_1\mathbf{B}-\mathbf{B}^2)\\&+2(\psi_4^*-I_1\psi_5^*)\mathbf{m}\otimes\mathbf{m}+2\psi_5^*(\mathbf{m}\otimes\mathbf{Bm}+\mathbf{Bm}\otimes\mathbf{m}),\end{aligned} \tag{2.8}$$

where $\psi_i^*=\partial\Psi^*/\partial I_i,\ i=1,2,4,\ \psi_5^*=\partial\Psi^*/\partial I_5^*$. In principle the four constitutive functions ψ_1,ψ_2,ψ_4 and ψ_5, equivalently $\psi_1^*,\psi_2^*,\psi_4^*$ and ψ_5^*, can be determined on the basis of four independent test protocols (see Holzapfel & Ogden 2009*c*); however, limitations of currently available experimental apparatus preclude the possibility of performing such tests simultaneously on a single specimen. Nevertheless, much valuable data can be obtained on the basis of planar biaxial tests on thin sheets of material, uniaxial tests on strips of tissue or from shear tests. In particular, we now describe a theory that provides the basis for analysing data from biaxial tests.

Biaxial extension of a thin sheet of tissue is a commonly used test protocol. For a thin sheet it is appropriate to adopt the membrane approximation, and with reference to Cartesian axes $\mathbf{e}_1$ and $\mathbf{e}_2$ aligned with the edges of the sheet and $\mathbf{e}_3$ normal to the plane of the sheet in the reference configuration the membrane

approximation is expressed through the equations $\sigma_{i3}=0$, $i=1,2,3$. The in-plane stresses are then (Holzapfel & Ogden 2009*c*)

$$\sigma_{11}=2(B_{11}-B_{33})\psi_1+2[(B_{11}-B_{33})B_{22}-B_{12}^2]\psi_2+2m_1^2\psi_4 + 4m_1(B_{11}m_1+B_{12}m_2)\psi_5, \tag{2.9}$$

$$\sigma_{22}=2(B_{22}-B_{33})\psi_1+2[(B_{22}-B_{33})B_{11}-B_{12}^2]\psi_2+2m_2^2\psi_4 + 4m_2(B_{12}m_1+B_{22}m_2)\psi_5 \tag{2.10}$$

and

$$\sigma_{12}=2B_{12}\psi_1+2B_{12}B_{33}\psi_2+2m_1m_2\psi_4+2[m_1m_2(B_{11}+B_{22}) + B_{12}(m_1^2+m_2^2)]\psi_5, \tag{2.11}$$

where B_{ij} are the components of $\mathbf{B}$, with $B_{13}=B_{23}=0$, and m_1 and m_2 are the components of $\mathbf{m}$, with $m_3=0$. Equations (2.9)–(2.11) contain the *four* independent constitutive functions ψ_1,ψ_2,ψ_4 and ψ_5. However, only *three* independent components of deformation are included in these equations, namely B_{11}, B_{22} and B_{12} (note that by the incompressibility condition B_{33} is given in terms of these three components). These are related to just *three* components of stress. It is not possible, therefore, to solve the equations uniquely for ψ_1,ψ_2,ψ_4 and ψ_5. Thus, planar biaxial tests alone are insufficient to fully characterize the elastic properties of the material.

In the specialization to pure homogeneous deformation the component matrix of $\mathbf{F}$ is diagonal with entries λ_1,λ_2 and λ_3, which are the principal stretches. We then have $B_{11}=\lambda_1^2$, $B_{22}=\lambda_2^2$ and $B_{12}=0$ and by use of the incompressibility condition, which yields $\lambda_3=\lambda_1^{-1}\lambda_2^{-1}$, equations (2.9)–(2.11) simplify to

$$\sigma_{11}=2(\lambda_1^2-\lambda_1^{-2}\lambda_2^{-2})(\psi_1+\lambda_2^2\psi_2)+2m_1^2\psi_4+4\lambda_1^2m_1^2\psi_5, \tag{2.12}$$

$$\sigma_{22}=2(\lambda_2^2-\lambda_1^{-2}\lambda_2^{-2})(\psi_1+\lambda_1^2\psi_2)+2m_2^2\psi_4+4\lambda_2^2m_2^2\psi_5 \tag{2.13}$$

and

$$\sigma_{12}=2m_1m_2[\psi_4+(\lambda_1^2+\lambda_2^2)\psi_5], \tag{2.14}$$

and in terms of the principal stretches the invariants become

$$I_1=\lambda_1^2+\lambda_2^2+\lambda_1^{-2}\lambda_2^{-2} \quad \text{and} \quad I_2=\lambda_1^{-2}+\lambda_2^{-2}+\lambda_1^2\lambda_2^2 \tag{2.15}$$

and

$$I_4=m_1^2+m_2^2 \quad \text{and} \quad I_5=\lambda_1^2m_1^2+\lambda_2^2m_2^2. \tag{2.16}$$

Note that since $B_{12}=0$ there is no shear deformation but in general the shear stress σ_{12} is non-zero unless either $m_1=0$ or $m_2=0$, in which case the fibre direction is aligned with one of the in-plane coordinate axes.

For some tissues, such as arterial wall tissues, two families of fibres can be distinguished. These are then associated with two distinct preferred directions in the reference configuration, and for the second one we denote the corresponding unit vector by $\mathbf{M}'$. This introduces three additional invariants; two are analogous to I_4 and I_5 and denoted I_6 and I_7, and the third is a coupling invariant which involves both $\mathbf{M}$ and $\mathbf{M}'$. These are defined by

$$I_6=\mathbf{M}'\cdot(\mathbf{C}\mathbf{M}'), \quad I_7=\mathbf{M}'\cdot(\mathbf{C}^2\mathbf{M}') \quad \text{and} \quad I_8=[\mathbf{M}\cdot(\mathbf{C}\mathbf{M}')](\mathbf{M}\cdot\mathbf{M}'). \tag{2.17}$$

Note that the factor $\mathbf{M}\cdot\mathbf{M}'$ in I_8 is included to ensure that I_8 does not depend on the sense of either $\mathbf{M}$ or $\mathbf{M}'$. The strain-energy function Ψ then depends (in general) on $I_1, I_2, I_4, I_5, I_6, I_7$ and I_8 for an incompressible material and we may associate with equation (2.17) three further constitutive functions ψ_6, ψ_7, ψ_8 defined by $\psi_i = \partial\Psi/\partial I_i$, $i = 6, 7, 8$. The corresponding expanded form of the Cauchy stress is not given here and we refer to, for example, Holzapfel (2000) or Ogden (2009) for the details. In this case there are seven constitutive functions and the six components of the (symmetric) Cauchy stress tensor $\boldsymbol{\sigma}$ are given in terms of the six components of the (symmetric) deformation tensor $\mathbf{B}$. These six connections are not enough to determine the seven constitutive functions uniquely, a similar situation to the case of transverse isotropy in relation to planar biaxial deformations.

The theoretical restriction alluded to above is to be considered in conjunction with the fact that data from a range of different deformations on particular tissues are scarce, and, indeed, there are insufficient data to be able to distinguish between the effects of the different deformation invariants via the constitutive functions. Therefore, in order to make the characterization of the material properties tractable it is usual practice to adopt some specialization of the functional dependence of Ψ, in particular by reducing its dependence on the number of invariants and hence reducing the number of constitutive functions. In the following subsection we examine some examples of this reduction and henceforth we restrict attention to incompressible materials.

(*b*) *Specific strain-energy functions*

Without loss of generality we may write the strain-energy function for a material with a single preferred direction $\mathbf{M}$ (with no dependence on the sense of $\mathbf{M}$) in the form

$$\Psi(\mathbf{C}, \mathbf{M}\otimes\mathbf{M}) = \Psi_{\mathrm{g}}(\mathbf{C}) + \Psi_{\mathrm{f}}(\mathbf{C}, \mathbf{M}\otimes\mathbf{M}) \tag{2.18}$$

by separating out part of Ψ that is independent of $\mathbf{M}$. Now, however, it is convenient to specialize this by associating Ψ_{g} with the non-collagenous ground substance (indicated by subscript g) and Ψ_{f} with the embedded family of collagen fibres (indicated by subscript f), as was originally proposed by Holzapfel & Weizsäcker (1998) and adopted subsequently by many authors. For the transversely isotropic case, equation (2.18) can be represented in terms of invariants as

$$\Psi(I_1, I_2, I_4, I_5) = \Psi_{\mathrm{g}}(I_1, I_2) + \Psi_{\mathrm{f}}(I_1, I_2, I_4, I_5). \tag{2.19}$$

A simple starting point, which captures both the isotropy of the ground substance through I_1 and the transverse isotropy associated with the fibres through I_4, is the reduced form

$$\Psi(I_1, I_4) = \Psi_{\mathrm{g}}(I_1) + \Psi_{\mathrm{f}}(I_4). \tag{2.20}$$

In order to relate this model to available experimental data, it is common practice to treat the ground substance as a neo-Hookean material and this can in part be justified by the study of Gundiah *et al.* (2007), which showed that the

neo-Hookean model gives a satisfactory description of the mechanical response of arterial elastin, an important constituent of the ground substance. Hence, we may take

$$\Psi_{\mathrm{g}}(I_1) = \frac{c}{2}(I_1 - 3), \tag{2.21}$$

where $c > 0$ is a stress-like parameter, which for the neo-Hookean material in isolation may be identified as the shear modulus of the material in the reference configuration.

The strong stiffening effect of the tissue observed at higher loadings is almost entirely due to collagen fibres and motivates the use of an exponential function for the description of the strain energy stored in the collagen fibres, as originally proposed by Fung (1967). Thus, as in Holzapfel *et al.* (2000*a*), we take

$$\Psi_{\mathrm{f}}(I_4) = \frac{k_1}{k_2}\{\exp[k_2(I_4 - 1)^2] - 1\}, \tag{2.22}$$

where $k_1 > 0$ is a stress-like material parameter and $k_2 > 0$ is a dimensionless parameter. An appropriate choice of k_1 and k_2 enables the histologically based assumption that the crimped collagen fibres have little influence on the mechanical response of the artery in the low loading domain under tension to be modelled. Because of the wavy (crimped) structure it is generally assumed that collagen is not able to support compression since the fibres would buckle under the smallest compressive load. It is therefore assumed that the fibres contribute to the strain energy in extension but not in compression. Hence in the model (2.20), the anisotropic term should contribute only when the fibres are extended, that is, when $I_4 > 1$, and hence when $I_4 \leq 1$ the response of the tissue is purely isotropic. This modelling assumption is not only physically based, but is also essential for reasons of stability and consistency with inequalities such as strong ellipticity, as discussed in, for example, Holzapfel *et al.* (2004). For the model (2.20) with equations (2.21) and (2.22) the Cauchy stress tensor (2.6) reduces to

$$\boldsymbol{\sigma} = -p\mathbf{I} + c\mathbf{B} + 4k_1(I_4 - 1)\exp[k_2(I_4 - 1)^2]\mathbf{m} \otimes \mathbf{m}. \tag{2.23}$$

For small strains the stress–strain response should be consistent with the linear theory of transverse isotropy, which for an incompressible material involves three independent elastic constants. In terms of the classical Voigt notation c_{ij} the independent constants are $c_{11} - c_{12}$ and $c_{11} + c_{33} - 2c_{13}$ and c_{44} when the third direction is the direction of transverse isotropy. According to Merodio & Ogden (2005) these constants are related to the first and second derivatives of Ψ evaluated in the reference configuration by

$$\psi_1 + \psi_2 = \tfrac{1}{4}(c_{11} - c_{12}), \tag{2.24}$$

$$\psi_1 + \psi_2 + \psi_5 = \tfrac{1}{4}c_{44} \tag{2.25}$$

and

$$\psi_{44} + 4\psi_{45} + 4\psi_{55} = \tfrac{1}{4}(c_{11} + c_{33} - 2c_{13} - 4c_{44}), \tag{2.26}$$

where $\psi_{ij} = \partial^2\Psi/\partial I_i \partial I_j$, $i, j \in \{4, 5\}$; see also Ogden (2009). The strong ellipticity condition requires that $c_{11} - c_{12} > 0$, $c_{11} + c_{33} - 2c_{13} > 0$ and $c_{44} > 0$, and the

positivity of the material constants c and k_1 is consistent with these inequalities and we note the connections

$$\tfrac{1}{4}(c_{11} - c_{12}) = c_{44} = c \quad \text{and} \quad c_{11} + c_{33} - 2c_{13} = c + 8k_1. \tag{2.27}$$

Since it involves only two independent constants the model consisting of the sum of equations (2.21) and (2.22) therefore reduces to a special form of transversely isotropic material in the linear specialization.

A simple counterpart of equation (2.20) for a material with two families of fibres may be written in the form

$$\Psi(I_1, I_4, I_6) = \Psi_{\mathrm{g}}(I_1) + \Psi_{\mathrm{f}}(I_4, I_6), \tag{2.28}$$

where I_6 represents the square of the stretch in the direction of the second family of fibres, as defined by equation $(2.17)_1$. A commonly used form of the energy function (2.28), an extension of equation (2.22) to the two-fibre case in which the two families have the same mechanical properties, is given by

$$\Psi(I_1, I_4, I_6) = \frac{c}{2}(I_1 - 3) + \frac{k_1}{2k_2} \sum_{i=4,6} \{\exp[k_2(I_i - 1)^2] - 1\}. \tag{2.29}$$

Note that when $I_4 = I_6$ this reduces to the sum of equations (2.21) and (2.22). Such a model is particularly appropriate for arteries because of the symmetrical helical arrangement of the collagen fibres, with their directions $\mathbf{M}$ and $\mathbf{M}'$ lying in the tangent plane of the artery wall and making equal angles with the artery axis. The associated Cauchy stress tensor is

$$\begin{aligned} \boldsymbol{\sigma} = &-p\mathbf{I} + c\mathbf{B} + 2k_1(I_4 - 1)\exp[k_2(I_4 - 1)^2]\mathbf{m} \otimes \mathbf{m} \\ &+ 2k_1(I_6 - 1)\exp[k_2(I_6 - 1)^2]\mathbf{m}' \otimes \mathbf{m}', \end{aligned} \tag{2.30}$$

generalizing equation (2.23), where $\mathbf{m}' = \mathbf{F}\mathbf{M}'$. This model is discussed in the following subsection in connection with the extension and inflation of an artery.

(*c*) *Application to the extension and inflation of an arterial segment*

Extension–inflation tests on arterial segments provide an alternative means of obtaining biaxial data. Let us consider an artery as a thick-walled circular cylindrical tube, which in its unloaded configuration has internal and external radii A and B, respectively, and length L. Its geometry may then be described in terms of cylindrical polar coordinates (R, Θ, Z) by $A \le R \le B$, $0 \le \Theta \le 2\pi$, $0 \le Z \le L$. The corresponding deformed tube, with the circular cylindrical symmetry maintained, is then described by cylindrical polar coordinates (r, θ, z), with $a \le r \le b$, $0 \le \theta \le 2\pi$, $0 \le z \le l$, where a, b and l are the deformed counterparts of A, B and L and the deformation is given by

$$r^2 = a^2 + \lambda_z^{-1}(R^2 - A^2), \quad \theta = \Theta \quad \text{and} \quad z = \lambda_z Z, \tag{2.31}$$

where $\lambda_z = l/L$ is the uniform stretch in the axial direction and the first equation is a consequence of the incompressibility condition. Because of the symmetry the component matrix of the deformation gradient with respect to the cylindrical axes is diagonal and its entries are again the principal stretches, which we write as $\lambda^{-1}\lambda_z^{-1}, \lambda, \lambda_z$ in the radial, azimuthal and axial directions, respectively, where λ is

the azimuthal stretch r/R and the radial stretch is given by the incompressibility condition. The deformation is locally biaxial in the (θ, z) tangential plane, with λ dependent on the radius.

Let φ denote the angle between each of the fibre directions $\mathbf{M}$ and $\mathbf{M}'$ and the circumferential direction so that they are symmetrically disposed with respect to the axis and have no component in the radial direction. Then, the invariants I_1, I_4 and I_6 can all be expressed as functions of the two independent stretches as

$$I_1 = \lambda^2 + \lambda_z^2 + \lambda^{-2}\lambda_z^{-2} \quad \text{and} \quad I_6 = I_4 = \lambda^2 \cos^2\varphi + \lambda_z^2 \sin^2\varphi, \tag{2.32}$$

and, for the considered deformation, Ψ can be regarded as a function of λ and λ_z, which we write as $\hat{\Psi}(\lambda, \lambda_z)$. By a standard calculation using the components of the Cauchy stress (2.30) we obtain the stress differences

$$\sigma_{\theta\theta} - \sigma_{rr} = \lambda \frac{\partial \hat{\Psi}}{\partial \lambda} \quad \text{and} \quad \sigma_{zz} - \sigma_{rr} = \lambda_z \frac{\partial \hat{\Psi}}{\partial \lambda_z}. \tag{2.33}$$

Because of the symmetry there is no shear stress and the normal stresses $\sigma_{rr}, \sigma_{\theta\theta}$ and σ_{zz} are principal stresses, and the equilibrium equation consists of just the radial equation

$$\frac{\mathrm{d}\sigma_{rr}}{\mathrm{d}r} + \frac{1}{r}(\sigma_{rr} - \sigma_{\theta\theta}) = 0. \tag{2.34}$$

A standard experimental protocol involves application of an internal pressure and an axial load to an arterial segment with closed ends. Let the internal pressure be denoted by P and the resultant axial load by N. Then, integration of equation (2.34) and application of the boundary conditions $\sigma_{rr} = -P$ on $r = a$ and $\sigma_{rr} = 0$ on $r = b$ leads to the expression

$$P = \int_a^b \lambda \frac{\partial \hat{\Psi}}{\partial \lambda} \frac{\mathrm{d}r}{r} \equiv \int_{\lambda_b}^{\lambda_a} (\lambda^2\lambda_z - 1)^{-1} \hat{\psi}_\lambda \, \mathrm{d}\lambda, \tag{2.35}$$

while, after some rearrangement using equation (2.34), the resultant axial load, given by

$$N = 2\pi \int_a^b \sigma_{zz} r \, \mathrm{d}r, \tag{2.36}$$

can be written in the form

$$F \equiv N - \pi a^2 P = \pi A^2 (\lambda_a^2 \lambda_z - 1) \int_{\lambda_b}^{\lambda_a} (\lambda^2\lambda_z - 1)^{-2} (2\lambda_z \hat{\psi}_{\lambda_z} - \lambda \hat{\psi}_\lambda) \lambda \, \mathrm{d}\lambda, \tag{2.37}$$

where F is the so-called reduced axial force (the force applied in the axial direction additional to that generated by the pressure on the closed ends of the tube), $\hat{\psi}_\lambda = \partial\hat{\Psi}/\partial\lambda$, $\hat{\psi}_{\lambda_z} = \partial\hat{\Psi}/\partial\lambda_z$ and λ_a and λ_b are the values of λ at $r = a$ and $r = b$, respectively. For detailed derivation of the formulae (2.35) and (2.37) see, for example, Ogden (2009). In this connection, we note that it can be shown from equation (2.31) that

$$\lambda^2\lambda_z - 1 = \frac{(\lambda_a^2\lambda_z - 1)A^2}{R^2} \tag{2.38}$$

and hence that $\lambda^2\lambda_z - 1$ has the same sign throughout the wall thickness.

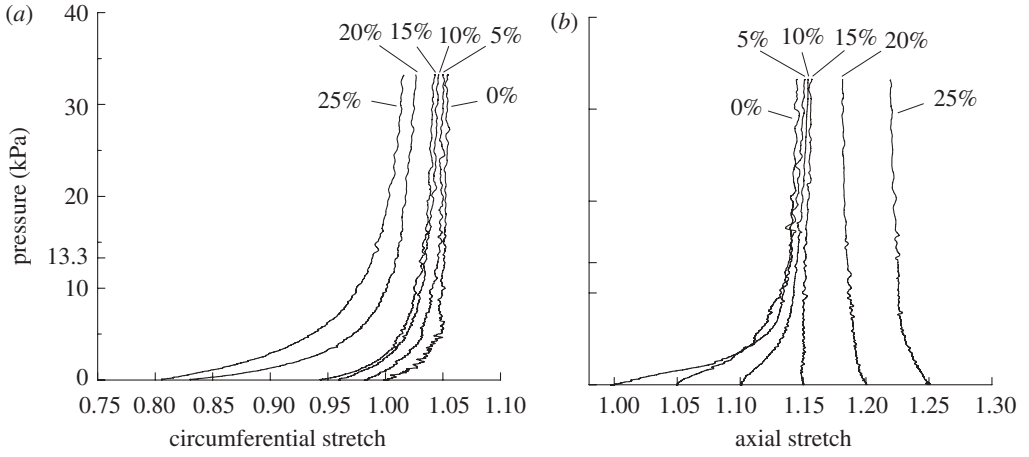

Figure 1. Representative pressure–stretch response of an intact internal carotid artery. (*a*) Pressure versus circumferential stretch for fixed values of the axial stretch. (*b*) Pressure versus axial stretch for different starting values of the axial stretch. Modified from Sommer *et al.* (2010).

For a thin-walled tube, the formulae (2.35) and (2.37) can be approximated by

$$P = \varepsilon\lambda^{-1}\lambda_z^{-1}\hat{\psi}_\lambda \quad \text{and} \quad F = \varepsilon\pi A^2(2\hat{\psi}_{\lambda_z} - \lambda\lambda_z^{-1}\hat{\psi}_\lambda), \tag{2.39}$$

where $\varepsilon = (B - A)/A$.

The first part in equation (2.39) provides the theoretical background against which the representative data from the recent study by Sommer *et al.* (2010), shown in figure 1, may be discussed. In particular, in figure 1*a* the internal pressure is plotted as a function of the circumferential stretch for several fixed values of the axial stretch. These curves show the characteristic stiffening response associated with the stretching of the collagen fibres following the relatively soft response primarily associated with the deformation of the ground substance. As can be seen, the response is stiffer for higher axial pre-stretches. For other types of soft tissues, such as the myocardium, a similar stiffening response can be observed (e.g. Dokos *et al.* 2002). Figure 1*b* shows the pressure as a function of the axial stretch starting from an initial axial pre-stretch at zero pressure. These plots show that the arterial tube elongates during inflation for low axial pre-stretches, but for larger axial pre-stretches the tube length decreases with pressure. The transition between these two behaviours corresponds to an axial pre-stretch of about 1.15, for which there is no change in length due to changes in pressure. This behaviour is typical for human arteries, as exemplified in Schulze-Bauer & Holzapfel (2003).

It should be emphasized that the data in figure 1 are for an intact internal carotid artery. The behaviours of the constituent layers are quite different, and we illustrate this in figures 2 and 3, where the behaviour of each of the media–intima composite and the adventitia is shown for the same artery on the same basis as in figure 1. From figure 2, we highlight two features: with reference to figure 2*a* the initial axial stretch has a negligible effect on the circumferential stretch and it has only a small influence on the pressure versus circumferential

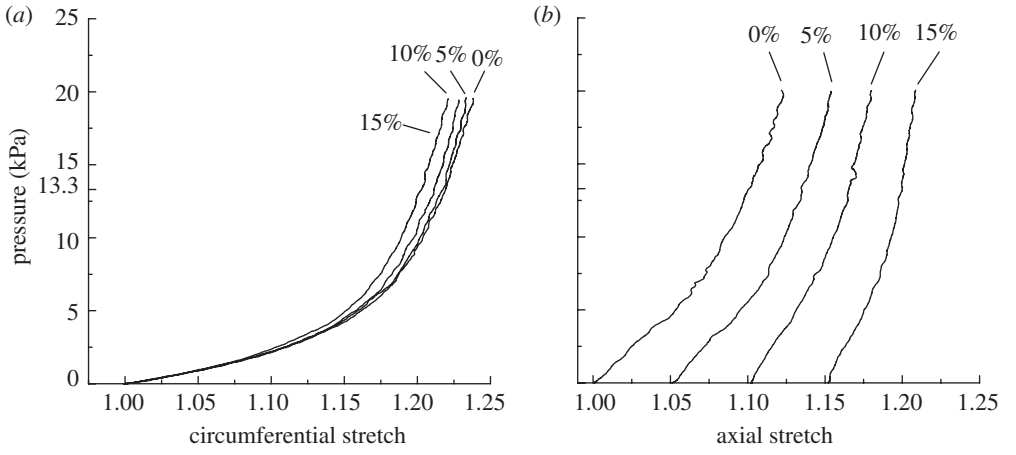

Figure 2. Representative pressure–stretch response of the media–intima composite of an internal carotid artery. (*a*) Pressure versus circumferential stretch for fixed values of the axial stretch. (*b*) Pressure versus axial stretch for different starting values of the axial stretch. The media–intima composite is from the same artery as in figure 1. Modified from Sommer *et al.* (2010).

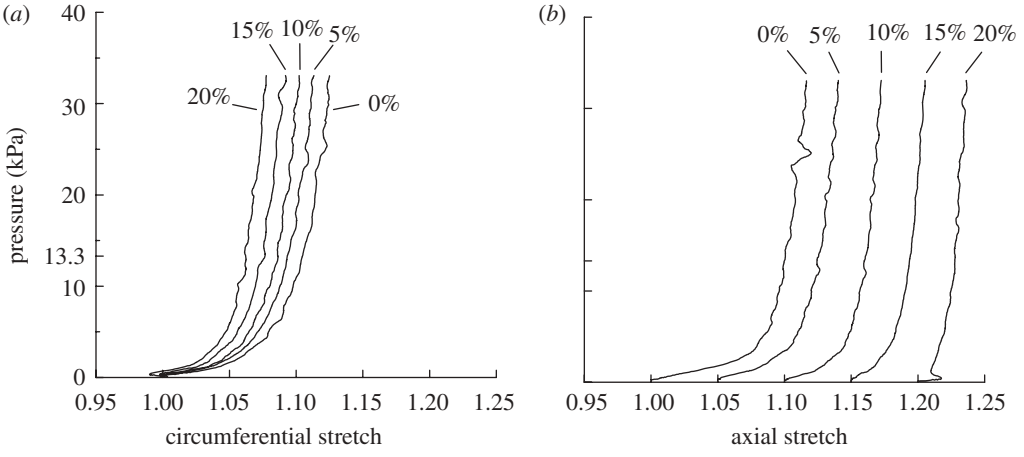

Figure 3. Representative pressure–stretch response of the adventitia of an internal carotid artery. (*a*) Pressure versus circumferential stretch for fixed values of the axial stretch. (*b*) Pressure versus axial stretch for different starting values of the axial stretch. The adventitia is from the same artery as in figure 1. Modified from Sommer *et al.* (2010).

stretch plot for the range of axial stretches achieved. The inversion characterized in figure 1*b* does not appear because the axial stretches reached were not as large as those for the intact artery. In the case of the adventitia, as shown in figure 3, the influence of the initial axial stretch was slightly more noticeable for zero pressure, and the pressure response was more dependent on the axial stretch (see figure 3*a*). From figure 3*b* we again see that there is no inversion effect within the considered elastic range up to 20 per cent axial stretch. Further

stretching was precluded because of the onset of damage and ultimate rupture of this layer. As can be seen from figure 3 the pressure–stretch behaviour of the adventitia stiffens more rapidly than for the media–intima composite shown in figure 2. Similar experimental data and ultimate tensile stresses and stretches from the individual layers of non-stenotic human left anterior descending coronary arteries are documented in Holzapfel *et al.* (2005*a*). This study showed the need to model non-stenotic human coronary arteries as structures composed of three solid mechanically relevant layers exhibiting distinct mechanical properties.

3. Applications of the fibre–structure model

Modelling of soft tissues as fibre-reinforced elastic materials on the basis of the invariant structure outlined in §2 is now well established and widely used. The main application to date has been in the context of arterial wall mechanics but it is also being used for a growing range of other tissues. In this section therefore we focus first on describing the different aspects of the use of the invariant approach for arteries but we then go on to discuss, albeit more briefly, some applications to other tissues and then more general applications to soft tissues not specific to particular tissues.

(*a*) *Arterial wall modelling and its applications*

An excellent starting point for the discussion of the mechanics of arteries and more generally of the cardiovascular system is the text by Humphrey (2002), wherein the basic constitutive structure for the description of the mechanics of arterial walls is developed. This includes a review of strain-energy functions available in the literature up to the year 2000, which are based mainly on the Fung model (see Humphrey 2002, §7.5). Discussion of more recent contributions can be found in the lecture notes edited by Holzapfel & Ogden (2003, 2009*a*) and the conference proceedings volume edited by Holzapfel & Ogden (2006). In the present section we focus on the development since 2000 of invariant-based structural models of arterial walls because they have been widely used in the literature since then and it has been recognized that this provides a general framework on which to build more sophisticated models.

We begin by considering the modelling of healthy arteries. The structurally based three-dimensional constitutive model developed by Holzapfel *et al.* (2000*a*, 2004) accounts for the collagen fibre orientation of each layer in the artery and for residual stresses and fits representative experimental data on different arteries. Moreover, it involves a relatively small number of material parameters and is consistent with requirements of material stability and mathematical considerations such as convexity and strong ellipticity. Figure 4 shows the deformation behaviour of a carotid artery during inflation and torsion modelled as a two-layer thick-walled tube (media, adventitia) with residual strains. The same form of constitutive model (2.29) was adopted for the two layers but a different set of material parameters was used for each layer. In particular, based on equations (2.35) and (2.37), respectively, the internal pressure P (figure 4*a*) and the reduced axial force F (figure 4*b*) are shown as functions of the internal radius a. In addition, the dependence of the torsional couple M_t

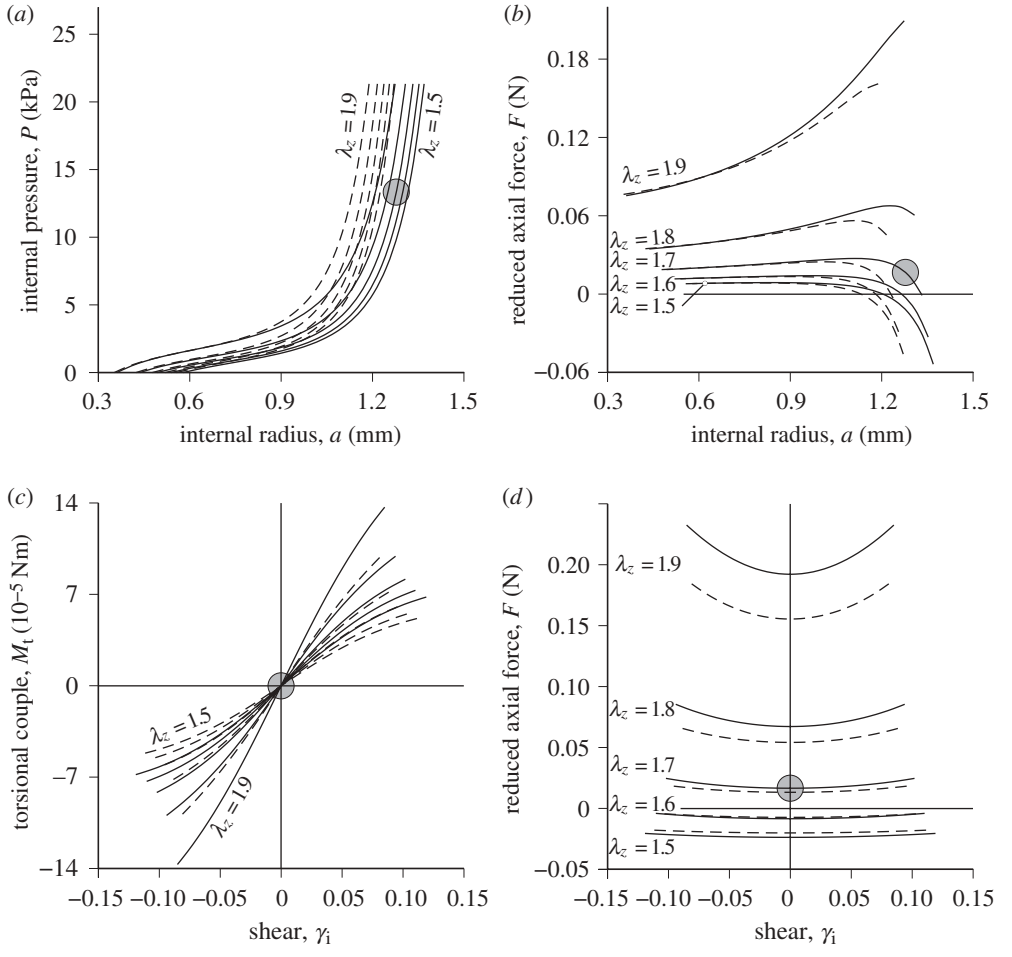

Figure 4. Deformation behaviour of a carotid artery during inflation and torsion using the constitutive model (2.29). Solid curves are numerical results with residual strains included ($\alpha = 160.0°$) and the dashed curves are results without residual strains. Dependence of (a) the internal pressure P and (b) the reduced axial force F on the internal radius a, without shear deformation ($\gamma_i = 0$). Dependence of (c) the torsional couple M_t and (d) the reduced axial force F on the shear γ_i at fixed internal pressure $P = 13.33$ (kPa). The shaded circles indicate the approximate central region of the physiological state. Reproduced from Holzapfel *et al.* (2000*a*) with kind permission of Springer Science and Business Media.

(figure 4*c*) and the reduced axial force F (figure 4*d*) on the shear γ_i at fixed internal pressure $P = 13.33$ (kPa) are depicted. A method for determining the parameters in this model on the basis of clinically registered pressure–radius signals was discussed by Stålhand (2009), who treated the artery as a single-layered membrane. The method developed was shown to be robust and yielded unique values of the material parameters. A similar approach using the same model was used by Masson *et al.* (2008). An extension of the model to include viscoelastic effects applied to examples of an artery under static and dynamic boundary loading conditions is documented in Holzapfel *et al.* (2002*a*). This

model captures the typical viscoelastic properties of muscular arteries, which are essentially insensitive to strain rate over several decades (nearly constant damping, independent of frequency).

Within the constitutive framework for elastic arteries described above the un-crimping of collagen fibres has been accounted for by use of an engagement strain described in terms of a probability distribution function (Zulliger *et al.* 2004*a*). This model captures the actual unfolding of the collagen fibres but has the disadvantage that the energy function associated with the fibres involves an integral over the probability distribution, which makes the model difficult to implement efficiently into numerical codes and therefore limits its applicability. An engagement strain was also discussed by Speirs *et al.* (2008), who used a finite element implementation to analyse the inflation and extension of a thick-walled tube by using the models (2.21) and (2.22) and compared the results with those from the engagement model of Zulliger *et al.* (2004*a*).

Baek *et al.* (2007*a*), Hu *et al.* (2007) and Zeinali-Davarani *et al.* (2009) considered a model of the form of equation (2.29) but with four families of fibres instead of two. This model is motivated by microscopic data on the arterial collagen organization obtained from multi-photon microscopy (Wicker *et al.* 2008). The additional two families, with equal material properties, are said to describe the properties of fibres oriented in the circumferential and axial directions. Gasser *et al.* (2002) and Chen *et al.* (2009) used the model (2.29) in applications to the analysis of wall stresses and strains during the clinically relevant procedure of arterial clamping. The first of these papers adopted a two-layer model for the media and adventitia and showed, in particular, that the axial stress increased very significantly during the clamping procedure, while the second paper was concerned with fluid–structure interactions and used a single-layer model to evaluate the effect of clamping on the wall stresses.

We now turn attention to the modelling of arteries under pathological conditions and the related clinical procedure of balloon angioplasty. The papers by Tang *et al.* (2009) and Yang *et al.* (2009) describe three-dimensional fluid–structure interaction in human coronary arteries with atherosclerotic plaques using more advanced computational analysis. The solid model was based on equations (2.21) and (2.22) with an additional exponential function in I_1. One conclusion was that cyclic bending and anisotropic properties may cause an increase of between 50 and 800 per cent in the maximum principal stress values at selected locations. The model has also served as a basis for examination of the biaxial behaviour of carotid arteries from mice with muscular dystrophy (Gleason *et al.* 2008). The four-fibre family model provided a good fit to the passive data in this case.

The procedure of balloon angioplasty has received considerable attention in the literature from the point of view of modelling. The first layer-specific three-dimensional model of the mechanics of balloon angioplasty was developed by Holzapfel *et al.* (2002*b*) following a preliminary study documented by Holzapfel *et al.* (2000*b*). Figure 5*a* shows the distribution of the circumferential Cauchy stresses (in kPa) in a representative cross section of a highly stenotic external iliac artery (male, 68 years) in a configuration where the angioplasty balloon is fully expanded. The three-dimensional analysis was also based on the model (2.21) with (2.22) and included an extension to incorporate the inelastic effects that are

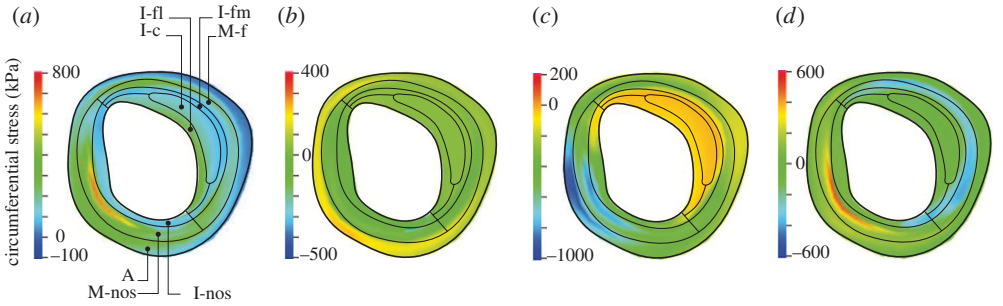

Figure 5. Plots of the circumferential stresses (in kPa) at a representative cross section of a highly stenotic artery in a loaded configuration corresponding to a fully expanded angioplasty balloon. The plots are superimposed on the geometry of the load-free configuration. Comparison of (*a*) reference simulation; (*b*)–(*d*) stress difference plots (reference model stresses minus simplified model stresses) for the three model simplifications, namely (*b*) neglecting axial *in situ* prestretch, (*c*) assuming plane strain and (*d*) isotropic material response. I-fl, collagenous cap (fibrotic part at the luminal border); I-fm, fibrotic intima at the medial border; I-c, calcification; M-f, diseased fibrotic media; I-nos, non-diseased intima; M-nos, non-diseased media; A, adventitia. Adapted from Holzapfel *et al.* (2002*b*).

evidenced during the high-pressure response of an artery (reference simulation in figure 5*a*); see also Holzapfel & Gasser (2007). The structural composition formed by the different tissues is distinguished by the associated boundary curves. Figure 5*b–d* shows circumferential stress difference plots, i.e. reference model stresses minus simplified model stresses. The model simplifications are characterized by, respectively, neglecting axial *in situ* prestretch, assuming a plane strain state, and isotropic material response. Since these simplifications led to maximum stress deviations of up to 600 per cent it was concluded that the associated models are in general inappropriate. The plots are superimposed on the load-free configuration. Inelastic effects that occur during the supra-physiological artery loading of angioplasty were also captured in the finite element model of Gasser & Holzapfel (2007*a*), which provided a detailed analysis of the stress distribution through the different layers. They pointed out that the three-dimensional stress states under physiological loading conditions before and after balloon inflation differ significantly and that even compressive normal stresses may occur in the media following dilation.

The study by Gasser & Holzapfel (2007*b*) models plaque fissuring and dissection during balloon angioplasty intervention on the basis of the model (2.29) for each of the intima, media and the adventitia, while the lipid pool is treated as a neo-Hookean material. Results suggest that the plaque fissures at both shoulders of the fibrous cap and stops at the lamina elastica interna and that dissections between the intima and the media develop, causing localized mechanical trauma, but protect the main portion of the stenosis from high stress and further tissue damage. In the paper by Kiousis *et al.* (2007), a more complex three-dimensional balloon–stent–artery interaction problem was modelled on the basis of the constitutive equation (2.29). The simulations analyse different stent designs, and a discussion of optimal stent designs for clinically relevant parameters was provided. Rodríguez *et al.* (2008*a*) used the model (2.29) to

describe the mechanical behaviour of the balloon, for which reinforcing fibres were taken to run in the circumferential and axial directions, with different sets of material parameters for the two directions.

An abnormal growth of the cross section of an artery is associated with the development of an aneurysm. Aneurysms occur primarily in cerebral arteries and the aorta. On the basis of the multi-layer model of Kroon & Holzapfel (2008*b*), the study by Kroon & Holzapfel (2009) investigated the distribution of the elastic properties of cerebral aneurysm tissue identified by an inverse finite element analysis. The proposed algorithm is able to estimate the distribution and the resulting maximum principal stress at physiological loading with satisfactory accuracy. Another computational method for inverse analysis was introduced by Lu *et al.* (2007) and applied to a simple example of a fusiform aneurysm. Rodríguez *et al.* (2009) studied two patient-specific abdominal aortic aneurysm (abbreviated as AAA) geometries at 120 mm Hg in order to determine the wall stresses. They compared an isotropic model with the model (2.29) and a generalization of that model which we discuss later in the paper (in §4), and they analysed the significant differences in the predictions of the models. In order to develop a criterion for assessing the risk of AAA rupture, Rissland *et al.* (2009) considered fluid–structure interactions in patient-specific geometries with and without intraluminal thrombus (ILT) using both an isotropic and an anisotropic material model. They determined the dependence of the wall stress distribution on the material model used with reference to the influence of ILT and concluded that an anisotropic model offers a more reliable predictor of AAA risk of rupture. A model that couples growth and rupture in AAA was developed by Volokh & Vorp (2008).

Also concerning arterial failure, Volokh (2007, 2008) investigated a criterion for failure of arteries during inflation using a two-layer model (media and adventitia) on the basis of a stress-softening function combined with equation (2.29). In addition, Gasser & Holzapfel (2006*b*) developed a three-dimensional cohesive-zone model to analyse dissection in a human artery. The computational results were compared with experimental data from Sommer *et al.* (2008), yielding excellent agreement.

An important area which has attracted considerable attention in the last few years is related to growth and remodelling of tissues, with particular emphasis on artery walls in health and disease. We mention first those papers which make use of the model (2.29). These include the study by Rodríguez *et al.* (2007), who modelled volumetric growth due to shear wall stress on the inner wall. They developed a three-dimensional finite element implementation and illustrated the evolution of the maximum principal stress in a stenosis. In the work of Hariton *et al.* (2007*a*,*b*), a simple finite element-based and stress-modulated framework for collagen fibre remodelling in artery walls was postulated. Their simulation for a human common carotid artery predicts a fibre morphology that correlates well with experimental observations. The proposed algorithm is also able to predict a fibre architecture in a human carotid bifurcation that correlates well with histological observations reported by Finlay *et al.* (1998).

In the paper by Alford *et al.* (2008), a mathematical model for growth and remodelling of arteries was presented for a thick-walled tube composed of a constrained mixture of smooth muscle cells, elastin and collagen within the framework developed by Humphrey & Rajagopal (2002) in combination with the

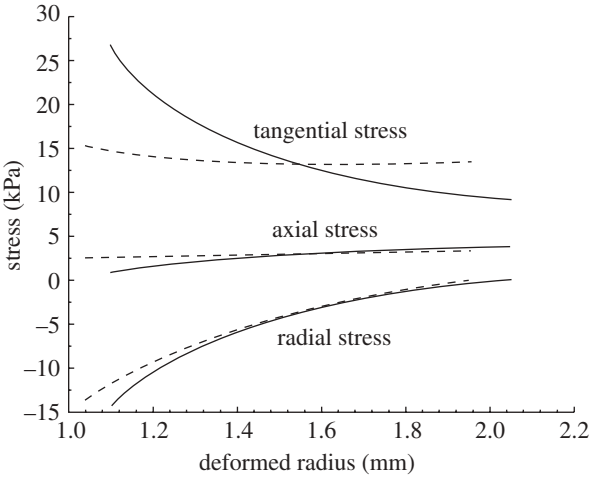

Figure 6. First Piola–Kirchhoff stress in the initial loaded configuration (solid curves) and in the grown configuration (dashed curves) through the deformed radius of a thick-walled cylinder. Reprinted from Olsson & Klarbring (2008) with permission from Elsevier.

kinematic growth model of Rodriguez *et al.* (1994). Predicted pressure–radius relations and opening angles show reasonable agreement with the experimental results from the literature. A variant of the model using a (discretized) Gaussian distribution for the fibre orientation concentration, documented by Driessen *et al.* (2008), analyses the evolution of the mean fibre direction and the dispersion about that direction in an arterial wall and in an aortic valve. The remodelling law for the collagen architecture is based on that of Hariton *et al.* (2007*a*,*b*). For the arterial wall, the model is able to predict the development of two helically arranged families of collagen fibres. Olsson & Klarbring (2008) constructed a thermodynamically consistent model for growth and remodelling in elastic arteries and represented the interaction between the mechanics and the biochemical control system by configurational forces in energetic duality with growth and remodelling. The plots in figure 6 show the first Piola–Kirchhoff stresses through the deformed radius of a (single layer) thick-walled cylinder. The transmural tangential and axial stresses evolve towards a nearly constant value. The work by Valentín & Humphrey (2009) is based on evaluating the sensitivity of the predictions of the constrained mixture model of artery growth and remodelling to variations in parameters that relate to the rate of turnover of collagen fibres and smooth muscle in particular.

Discussion of growth and remodelling is particularly appropriate in the context of the development of aneurysms, and there are several approaches in the literature that aim to capture the growth and remodelling of aneurysms in cerebral arteries or abdominal aortas. Approaches that are based on the structural model of §2 are now briefly reviewed. Vena *et al.* (2008) proposed a time-dependent model for growth of cerebral aneurysms in which the growth process is the result of two competing mechanisms, specifically the changes in the collagen fibre reference length and in the collagen fibre density, governed by evolution laws. The two mechanisms were shown to have opposite effects on the stability

of tissue growth. Eriksson *et al.* (2009) modelled aneurysm growth in a human middle cerebral artery as a two-layer cylinder with the layers corresponding to the media and the adventitia. The aneurysm is regarded as a development of the adventitia following ideas from Kroon & Holzapfel (2007, 2008*a*), who suggested that the production and degradation of collagen fibres depends on the wall stretch. The anisotropy of the surrounding media was modelled using the strain-energy function (2.29). It was shown that an alteration in the axial *in situ* stretch of the artery has a significant effect on the steady-state shape of the aneurysm and the resulting stresses in the aneurysm wall.

A mathematical model describing the growth of an abdominal aortic aneurysm as a two-layer membrane was proposed by Watton *et al.* (2004). This uses the strain-energy function (2.29) adapted to incorporate variable recruitment and density of collagen fibres and so allowing the collagen to remodel during aneurysm growth. Watton & Hill (2009) extended this model in order to accommodate evolving mechanical properties which are clinically measurable and consistent with experimental observations reported by Länne *et al.* (1992). Another interesting application of equation (2.29), in which the anisotropic exponential terms have different material constants for the collagen fibres and smooth muscles, is to the analysis of the progression and resolution of vasospasm in the work of Baek *et al.* (2007*b*). The constitutive relations used combine information on the wall properties with haemodynamics and chemical kinetics, and the results are consistent with the main features of clinically reported vasospasm.

In the development of constitutive models, it is important to take account of their mathematical structure with particular reference to the prediction of a physically (in the present context biomechanically) reasonable response. This is particularly related to notions of convexity and strong ellipticity and to material stability, as was emphasized in the work by Holzapfel *et al.* (2000*a*, 2004) and in the lecture notes by Ogden (2003, 2009). Against this background a framework for the construction of anisotropic polyconvex models for soft biological tissues was presented by Balzani *et al.* (2006). In this paper predictions of the model (2.21) with (2.22) and polyconvex variants of the model are compared with experimental data from uniaxial extension tests on circumferential and axial strips obtained from the media of a human abdominal aorta.

(*b*) *Modelling other soft tissues*

The fibre–structure models that have been used so successfully for arterial tissue have also been used, in one variant or another, to describe the elastic properties of many other soft biological tissues. Those for which the invariant-based framework has been used include veins, intestine, oesophagus, cornea, intervertebral disc, ligament, cartilage and the myocardium, but this list in not exhaustive. Here we comment briefly on each of these.

An application to the passive behaviour of ovine infrarenal vena cava tissues was the subject of the paper by Alastrué *et al.* (2008*b*), in which the modelling approach was based on equation (2.29) but with different constants associated with I_4 and I_6. Their own experimental data showed the marked anisotropic character of the tissue, which was reproduced accurately with their model.

The intestinal wall is a fibrous tissue with a layered structure. The main structural layers are the submucosa, which is composed almost entirely of collagen with two families arranged in a uniformly oriented cross ply. The muscular layer consists essentially of circumferentially oriented muscle fibres surrounded by a muscular coat with longitudinally oriented muscle fibres. This has been modelled as a fibre-reinforced elastic material by Ciarletta *et al.* (2009) using an extension of the model (2.29) that accounts for the contributions of the muscle fibres.

Based on the same framework, a similar constitutive model was used to describe the mechanical properties of oesophageal tissue by Yang *et al.* (2006). As with the model in Zulliger *et al.* (2004*a*), they used an engagement stretch associated with the un-crimping of collagen fibres.

The strain-energy function (2.29), with the neo-Hookean term replaced by a Mooney–Rivlin term, was used to study the mechanical behaviour of the human cornea in healthy conditions and in the presence of keratoconus for increasing intraocular pressure in Pandolfi & Manganiello (2006). Exactly the same constitutive model was used in Alastrué *et al.* (2006) and Lanchares *et al.* (2008) for analysing surgical procedures such as photorefractive keratectomy and limbal relaxing incisions, and for analysing the palpation of the cornea (Niroomandi *et al.* 2008).

The constitutive model (2.29) was also successfully applied to the description of the biomechanical response of the annulus fibrosus in the human lumbar spine (Eberlein *et al.* 2001, 2004). The model is appropriate because a single lamellar of the annulus fibrosus exhibits marked nonlinearity, anisotropy and distinct regional fibre orientation (Holzapfel & Ogden 2006). In addition, several ligaments connecting vertebrae in the lumbar spine are found to be transversely isotropic and have been modelled accordingly by using the same model as above (Holzapfel & Stadler 2006).

Recently the model (2.21) with equation (2.22) has been used as the basis for describing cartilage morphology and its material response by incorporating the collagen fibre fabric (Pierce *et al.* 2009).

Within the same general framework an extension of the model to the passive mechanical response of the myocardium has been developed by Holzapfel & Ogden (2009*b*). The model embraces the (orthotropic) morphological structure of the myocardium and accounts for the muscle fibre direction and the myocyte sheet structure and fits very well the available simple shear data of Dokos *et al.* (2002). Figure 7, adopted from Holzapfel & Ogden (2009*b*), shows a comparison of the constitutive model with *simple shear* data (Dokos *et al.* 2002) obtained from tests that were conducted on cube-shaped specimens from different orientations within the passive ventricular myocardium from pig hearts. The pairs fs, fn and sn refer to the fibre-sheet, fibre-normal and sheet-normal planes, and the enclosing parentheses indicate the direction of shear within the plane; for example, (fs) indicates shear in the s direction in the fs plane. The plots highlight the orthotropic behaviour of the material.

The passive ventricular myocardium exhibits a regionally dependent and, as is clear from the plots, highly nonlinear behaviour, and it is most resistant to shear deformations that produce extension of the myocyte (f) axis in the fs and fn planes (the upper two curves).

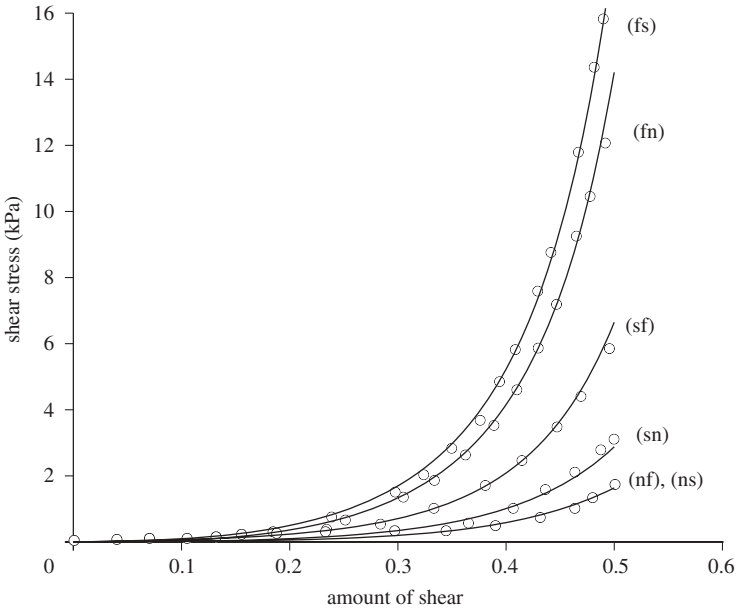

Figure 7. Fit of the constitutive model of Holzapfel & Ogden (2009*b*) to *simple shear* data obtained from tests that were conducted on cube-shaped specimens from the passive ventricular myocardium of pig hearts; see Dokos *et al.* (2002). The pairs fs, fn and sn refer to the fibre-sheet, fibre-normal and sheet-normal planes, and the direction of shear within each plane is identified by the ordered pair enclosed in parentheses, as described in the text. Open circle, experimental data; solid line, model. Reproduced from Holzapfel & Ogden (2009*b*).

It is worth highlighting here that for myocardial tissue in particular, but also for most other biological tissues, there is a shortage of consistent test data against which models can be reliably evaluated. There is thus a pressing need for more data.

(*c*) *Fibrous soft tissues in general*

Apart from its application discussed in the foregoing, the constitutive framework has also been used to analyse various general aspects of soft-tissue behaviour without reference to specific tissues. One example is in the paper by Karšaj *et al.* (2009), which considers time-dependent remodelling of fibre reorientation under certain boundary conditions using the transversely isotropic model (2.22) and the hypothesis that the fibres reorient towards a principal direction of stretch.

An extension to multi-layered structures with the mean fibre alignments distinguishing one layer from another was proposed in Kroon & Holzapfel (2008*b*). Particular examples of such a structure include artery walls, quadriceps tendons and airway walls.

Beyond purely elastic behaviour the model has been used within the context of viscoelasticity, damage and plasticity. Its extension to viscoelasticity is discussed in Holzapfel & Gasser (2001), which also includes computational implementation

and applications to simple boundary-value problems. A further extension to the mechanics of fibre-reinforced biological soft tissues to include three-dimensional finite-strain damage with viscoelasticity is documented in Peña *et al.* (2008*a*,*b*). The elastic part of the model used therein is a slight variant of equation (2.29).

A theoretical basis for including the model within the context of inelastic strains was provided in Gasser & Holzapfel (2002), which was also used in several applications, including those mentioned earlier, and allows for the possibility of multiple-fibre families.

Finally, we mention that this type of model has also been used for the analysis of textile composites, as illustrated in the papers by Nam & Thinh (2006) and Milani *et al.* (2007).

4. Modelling fibre dispersion

In several tissues there is a strong alignment of the collagen fibres with little dispersion in their orientation, but in other cases, such as in the adventitia of the artery wall, the heart valves and myocardial laminae, there is significant dispersion in the orientation, which has a significant influence on the mechanical response. It seems that the seminal paper by Lanir (1983) was the first to take account of fibre dispersion. This was accommodated by using a distribution density function for the fibre splay in connective tissues. However, because of the complexity of the model it has not proved to be a practical option for efficient numerical implementation. More recently models based on invariants have been adopted including those of Freed *et al.* (2005), Holzapfel *et al.* (2005*a*,*b*) and Gasser & Holzapfel (2006*a*). The model of Freed *et al.* (2005), for example, uses a structure tensor based on the Gaussian distribution of fibre directions for both two and three dimensions, and the model is applied to bioprosthetic valves; see also Freed (2008).

In what follows we discuss two other invariant-based models that account for fibre dispersion. For each model it is a minor operation to obtain the associated stress tensor and elasticity tensor, and finite element implementation of either model is straightforward and computationally efficient.

(*a*) *The* ρ *model*

The model of Holzapfel *et al.* (2005*a*,*b*) uses a strain-energy function of the form $\Psi(I_1, I_4) = \Psi_{\rm g}(I_1) + \Psi_{\rm f}(I_1, I_4)$, with

$$\Psi_{\rm f}(I_1, I_4) = \frac{k_1}{k_2}[\exp\{k_2[(1-\rho)(I_1-3)^2 + \rho(I_4-1)^2]\} - 1], \tag{4.1}$$

where $k_1 > 0$ and $k_2 > 0$ are stress-like and dimensionless parameters, respectively, to be determined from mechanical tissue tests. The parameter $\rho \in [0, 1]$ is a weighting factor between full isotropy and full alignment (transverse isotropy) and is therefore a measure of dispersion in the fibre orientation. The limit $\rho = 1$ corresponds to ideal alignment of collagen fibres (0% weight on the isotropic distribution), while in the limit $\rho = 0$ an isotropic distribution is obtained. In Holzapfel *et al.* (2005*a*) the model was shown to fit the layer-specific mechanical properties of human coronary arteries very well, while in Holzapfel *et al.* (2005*b*)

the model was related to the individual components of stenotic arteries and used to study the effect of angioplasty combined with stenting on the mechanical environment of the wall. The proposed methodology allows variations in a set of stent parameters that enables the difference in the mechanical environment within the wall before and after angioplasty with stenting to be evaluated.

A slight variant of equation (4.1), due to Rodríguez *et al.* (2008*b*), is

$$\Psi_{\mathrm{f}}(I_1, I_4) = \frac{k_1}{k_2}[\exp\{k_2[(1-\rho)(I_1-3)^2 + \rho(I_4 - I_4^0)^2]\} - 1], \tag{4.2}$$

where $I_4^0 > 1$ is a dimensionless parameter that is interpreted as a threshold value of I_4 beyond which the collagen fibres are un-crimped, and the anisotropic term therefore contributes only when $I_4 > I_4^0$. This model accurately captures the strong stiffening of collagenous tissue.

The model (4.1) served as a basis for the simulation of coronary artery bypass graft surgery, where the artery was modelled as a three-layer thick-walled tube and the finite element method was employed to predict the deformation and stress distributions at various stages of surgery (Cacho *et al.* 2007). It was found that the incision length has a critical influence on the graft shape and the stress in the graft wall, and that changes in the mechanical environment are severe, with stress concentrations occurring at the incision ends. Based on the same constitutive framework, Mortier *et al.* (2010) investigated and compared three different second-generation drug-eluting stents during implantation in the curved main branch of a coronary bifurcation in order to obtain insight into the changes of the mechanical environment. It turns out that the resulting distributions of the wall stresses are strongly dependent on the stent design, and it was shown how a stent design should be modified to reduce the maximum wall stresses. In addition, Kiousis *et al.* (2009) proposed a computational methodology to analyse the effect of changes in the lipid pool and calcification on wall stresses and on the collagenous cap vulnerability in a human carotid bifurcation. They found a positive correlation between the increase of lipid pool and the mechanical stress in the collagenous cap, and hence an increased risk of cap rupture. As a result of their analysis these authors were able to propose a novel vulnerability index to assess the risk of collagenous cap rupture. Figure 8 shows the distributions of the maximum principal Cauchy stress in the deformed configurations of characteristic cross sections in a carotid bifurcation at 140 mm Hg. In the reference model RM, the plaque volume consists of 25 per cent lipid pool I-lp and 75 per cent calcification I-c, while in a modified model MM these plaque-forming tissues are interchanged. In both models the highest stresses are identified at the thinnest part of the non-diseased wall, in the vicinity of the shoulders of the collagenous cap and in the calcification. Figure 8*c* shows the stress differences between these models and highlights the fact that for the internal carotid artery (ICA) the stress inside the collagenous cap I-fl for model MM is almost 50 kPa larger than that for model RM, thus indicating a more rupture-prone stenosis.

The two papers of Rodríguez *et al.* (2008*a*, 2009) analyse AAAs using models based on equations (4.1) and (4.2). In particular, in Rodríguez *et al.* (2008*b*), it is shown that with the modified model (4.2) a very good agreement with biaxial stress–stretch data from AAAs provided by Vande Geest *et al.* (2004) can be obtained. The results suggest that shorter aneurysms are more critical when

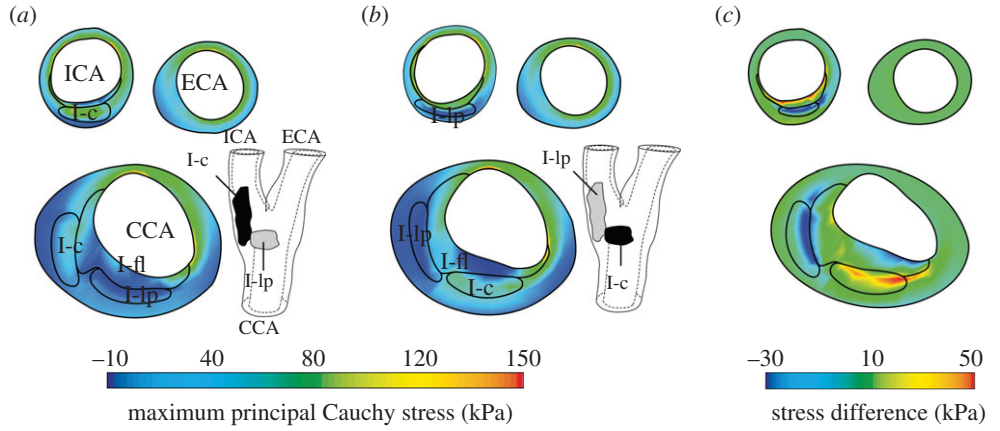

Figure 8. Maximum principal Cauchy stress in the deformed configurations of characteristic cross sections in a stenotic human carotid bifurcation (ICA, internal carotid artery; ECA, external carotid artery; CCA, common carotid artery) at a blood pressure of 140 mm Hg. (*a*) Reference model RM where the volume of the lipid pool I-lp constitutes 25% of the plaque volume and the volume of the calcification I-c constitutes the remaining 75%. (*b*) Modified model MM where the material models and parameters of the plaque-forming tissues (I-lp and I-c) are interchanged; stress difference between the models MM and RM in the unloaded configuration of the considered cross sections (*c*). For the sake of clarity, the boundaries of the collagenous cap I-fl, then I-lp and I-c are shown. Adapted from Kiousis *et al.* (2009).

asymmetries are present and they show the strong influence of anisotropy on the magnitude and distribution of the peak wall stress in AAAs. Rodríguez *et al.* (2009) compare the models (2.29) and (4.2) and an isotropic model on the basis of two patient-specific AAA geometries.

Modelling and analysis of the mechanical behaviour of mitral valves with their attached chordae tendineae on the basis of the models (4.1) and (4.2) was conducted by Prot *et al.* (2007, 2010) and Prot & Skallerud (2009). An application to a membrane shell using a finite element implementation was illustrated, and a comparative study of healthy and diseased valves was documented. In Prot & Skallerud (2009) it was shown that if the leaflet is modelled as a layered structure using layers with different material properties then the stresses in the fibre direction and the resistance to bending are reduced. The model (4.1) was used by Alastrué *et al.* (2008*a*) in the context of the modelling of adaptive growth of arteries with residual stresses incorporated.

(*b*) *The κ model*

The model of Gasser *et al.* (2006) is based on a generalized structure tensor $\mathbf{H}$ defined by

$$\mathbf{H} = \frac{1}{4\pi}\int_{\omega} \rho \mathbf{M}\otimes\mathbf{M}\,\mathrm{d}\omega, \tag{4.3}$$

which is the mean of the structure tensor $\mathbf{M}\otimes\mathbf{M}$ over the unit sphere ω weighted by the orientation distribution density ρ (not to be confused with the ρ in the previous subsection), where $\mathbf{M}$ is the local fibre direction and ρ is normalized

according to

$$\frac{1}{4\pi}\int_{\omega}\rho\,\mathrm{d}\omega = 1. \tag{4.4}$$

Clearly, $\mathbf{H}$ is symmetric and in general it has five independent components since, by equation (4.4), $\mathrm{tr}\mathbf{H} = 1$. Here, however, we consider only the case of a transversely isotropic distribution $\rho = \rho(\Theta)$, for which $\mathbf{H}$ involves only a single constant and is given by

$$\mathbf{H} = \kappa\mathbf{I} + (1-3\kappa)\overline{\mathbf{M}}\otimes\overline{\mathbf{M}} \quad \text{and} \quad \kappa = \frac{1}{4}\int_0^{\pi}\rho\sin^3\Theta\,\mathrm{d}\Theta, \tag{4.5}$$

where κ is a dispersion parameter, $\overline{\mathbf{M}}$ is the mean fibre direction and Θ is the angle between $\mathbf{M}$ and $\overline{\mathbf{M}}$. In this case equation (4.4) becomes $\int_0^{\pi}\rho\sin\Theta\,\mathrm{d}\Theta = 2$. Associated with $\mathbf{H}$ we define the invariant I_4^* as $\mathrm{tr}(\mathbf{CH})$ which, by equation $(4.5)_1$, yields

$$I_4^* = \kappa I_1 + (1-3\kappa)I_4, \tag{4.6}$$

where $I_4 = (\mathbf{C}\overline{\mathbf{M}})\cdot\overline{\mathbf{M}}$. The κ model is a strain-energy function of the form $\Psi(I_1, I_4) = \Psi_{\mathrm{g}}(I_1) + \Psi_{\mathrm{f}}(I_1, I_4)$ with

$$\Psi_{\mathrm{f}}(I_1, I_4) = \frac{k_1}{k_2}\{\exp[k_2(I_4^*-1)^2]-1\}, \tag{4.7}$$

where $k_1 > 0$ and $k_2 > 0$ are again stress-like and dimensionless material parameters, respectively.

(i) *The influence of the dispersion parameter* κ

In the paper by Gasser *et al.* (2006) the range of the dispersion parameter κ was considered to be $[0, \frac{1}{3}]$. The limits $\kappa = 0$ and $\frac{1}{3}$ correspond, respectively, to no dispersion (transverse isotropy) and a three-dimensional isotropic distribution of fibre orientation. It was pointed out by Li & Robertson (2009), however, that the absolute upper limit on κ is $\frac{1}{2}$. It is therefore interesting to consider the effect of values of κ between $\frac{1}{3}$ and $\frac{1}{2}$, and for this purpose we consider again the von Mises distribution in the form

$$\rho(\Theta) = 4\sqrt{\frac{b}{2\pi}}\frac{\exp[b(\cos(2\Theta)+1)]}{\mathrm{erfi}(\sqrt{2b})}, \tag{4.8}$$

where b is the so-called concentration parameter associated and $\mathrm{erfi}(x) = -\mathrm{i}\,\mathrm{erf}(\mathrm{i}x)$ denotes the so-called imaginary error function (Weisstein 2010), the error function itself being given by the standard formula

$$\mathrm{erf}(x) = \frac{2}{\sqrt{\pi}}\int_0^x \exp(-t^2)\,\mathrm{d}t. \tag{4.9}$$

If $b \geq 0$ then κ is restricted to the range 0 to $\frac{1}{3}$; however, the right-hand side of equation (4.8) is also real for $b < 0$ and then it is easy to show that the range of values $-\infty$ to $+\infty$ for b corresponds to $\kappa \in [0, \frac{1}{2}]$. A plot of the (monotonic) relationship between b and κ is shown in figure 9. For a set of values of κ within

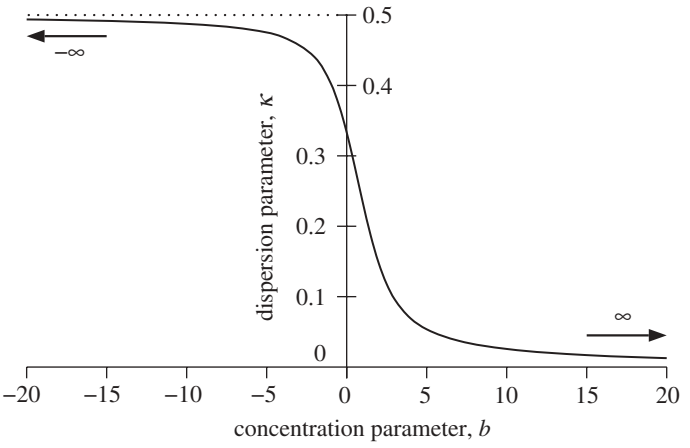

Figure 9. Plot of the concentration parameter b against the dispersion parameter κ based on the combination of equations $(4.5)_2$ and (4.8).

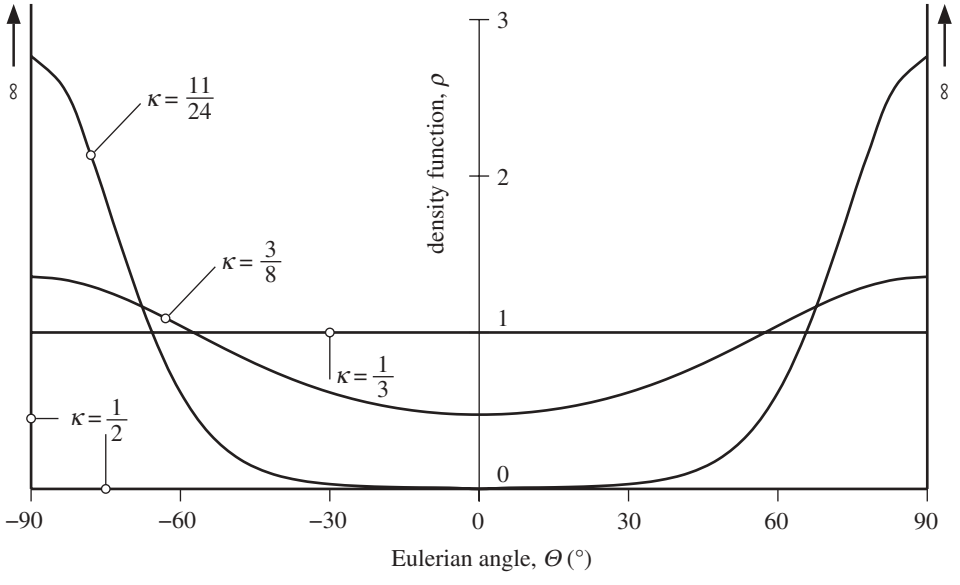

Figure 10. Plot of the (transversely isotropic) von Mises density function (4.8) against Θ with the centre shifted to $\Theta = 0$ for κ between $\frac{1}{3}$ and $\frac{1}{2}$ corresponding to a negative concentration b.

the range $[0, \frac{1}{3}]$ plots of the density function $\rho(\Theta)$ were shown by Gasser *et al.* (2006). Here, in figure 10, we show a corresponding plot of $\rho(\Theta)$ versus Θ centred on $\Theta = 0$ for $\frac{1}{3} \leq \kappa \leq \frac{1}{2}$, with $\kappa > \frac{1}{3}$ corresponding to 'negative concentration' b. This shows that the fibres are dispersed towards the peripheral angles.

In the limiting case $\kappa = \frac{1}{2}$ we have from equation (4.6)

$$I_4^* = \tfrac{1}{2}(I_1 - I_4), \tag{4.10}$$

which corresponds to a planar isotropic distribution of fibres with a preferred direction normal to that plane. Figure 11 shows a graphical representation of the surface of revolution about the mean fibre direction defined by the density function $\rho(\Theta)$, analogous to fig. 4 in Gasser *et al.* (2006), but for seven different fibre distributions, corresponding to $\kappa = 0$, $\frac{2}{15}$, $\frac{4}{15}$, $\frac{1}{3}$, $\frac{3}{8}$, $\frac{11}{24}$ and $\frac{1}{2}$.

As indicated above, the lower limit $\kappa = 0$ corresponds to all the fibres directed in the same direction, $\kappa = \frac{1}{3}$ provides an isotropic three-dimensional distribution, while the upper limit $\kappa = \frac{1}{2}$ gives an isotropic distribution in the plane normal to the preferred direction. For representation purposes the surfaces shown in figure 11 are scaled differently. As κ increases from $\frac{1}{3}$ to $\frac{1}{2}$ the fibre distribution becomes flatter and flatter, spreading towards the peripheral angles and in the limit it becomes planar, extending to infinity. Hence, the distribution changes from one-dimensional to three-dimensional down to two-dimensional.

As an illustration of the effect of values of κ between $\frac{1}{3}$ and $\frac{1}{2}$ we consider the pressure–stretch behaviour of a thin-walled circular cylindrical tube with two families of fibres distributed tangentially to the cylinder and symmetrically disposed with respect to the axis. The mean orientation of each family is at angle φ relative to the circumferential direction, as described in §2*c*. The plots in figure 12 show the relation between the dimensionless internal pressure $P^* = P/c\varepsilon$ and the circumferential stretch λ for a thin-walled (membrane) with the axial stretch $\lambda_z = 1$ calculated on the basis of equation $(2.39)_1$, where c is the material constant introduced in equation (2.21). The plots are based on the strain-energy function

$$\Psi = \frac{c}{2}(I_1 - 3) + \frac{k_1}{k_2}\{\exp[k_2(I_4^* - 1)^2] - 1\}, \tag{4.11}$$

where $I_4^* = \kappa I_1 + (1 - 3\kappa)I_4$ and I_1 and I_4 are given by equation (2.32), and are for different mean fibre orientations described by the angle φ and for $\kappa = 0, 0.226$, $\frac{1}{3}$ and $\frac{1}{2}$. As can be seen from figure 12 the mechanical response is stiffest for an isotropic material assumption and it is weakened by the dispersion. For $\kappa = \frac{1}{2}$ it is significantly weaker for $\varphi = 45°$ and $\varphi = 30°$, and we note that the ordering of the curves for the different angles for $\kappa > \frac{1}{3}$ is the opposite of that for $\kappa < \frac{1}{3}$. What is not clear from figure 12*a* is that the $\kappa = \frac{1}{2}$ curves are non-monotonic, and in some cases yield negative values of the pressure during the tube inflation. To clarify this the curves for small values of the pressure are shown on an enlarged scale in figure 12*b*. Clearly, values of κ between $\frac{1}{3}$ and $\frac{1}{2}$ yield undesirable effects and such values are therefore inappropriate for use in the present context of modelling soft tissues.

Note that for an incompressible material $I_1 \geq 3$, while if the mean fibre direction is stretched we have $I_4 \geq 1$. Then, provided $0 \leq \kappa \leq \frac{1}{3}$, we have $I_4^* \geq 3\kappa + (1 - 3\kappa) = 1$. However, if $\frac{1}{3} < \kappa \leq \frac{1}{2}$ then it is possible that $I_4^* < 1$, as we illustrate below.

As in §2*c* we now consider equation (4.11) as a function of λ and λ_z: $\hat{\Psi}(\lambda, \lambda_z)$. For the problem of extension and inflation of a thick-walled circular cylindrical tube the inflating internal pressure P is given by equation (2.35). We now investigate the sign of the integrand in equation (2.35), which, from

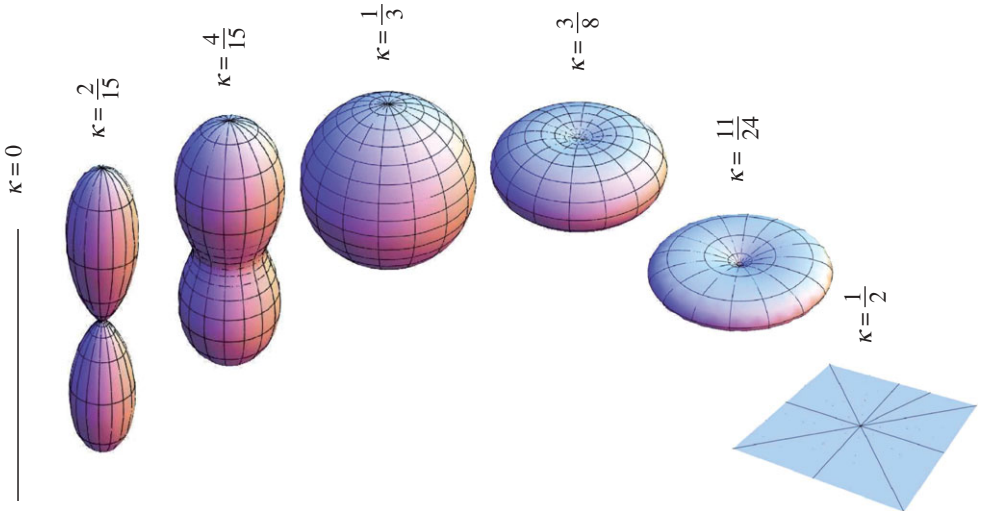

Figure 11. Three-dimensional graphical representation of the orientation density of the collagen fibres based on the transversely isotropic density function (4.8) for a representative set of values of the dispersion parameter κ.

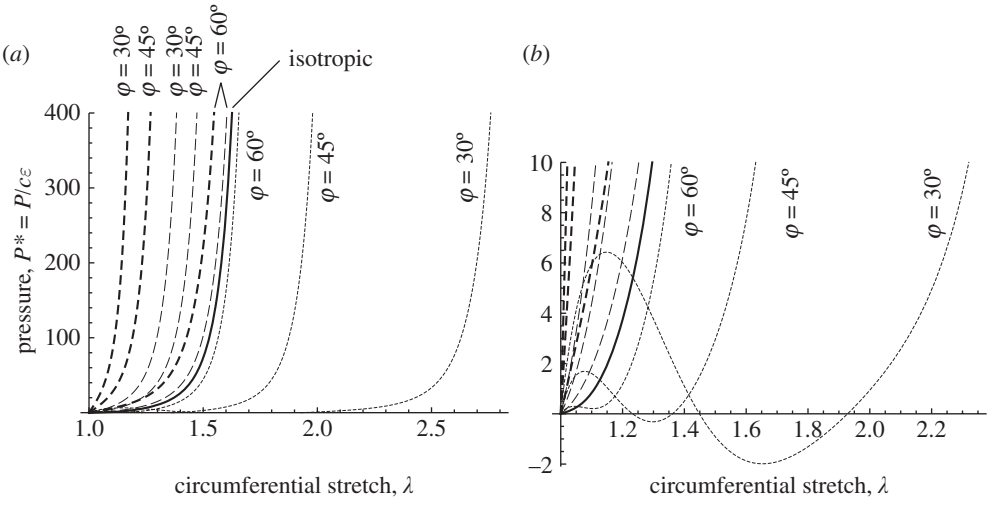

Figure 12. Plot of the dimensionless pressure $P^* = P/c\varepsilon$ against the circumferential stretch λ for fixed axial stretch $\lambda_z = 1$ for the constitutive model (4.11) using the formula $(2.39)_1$ and representative parameter values; $\kappa = 0$ is the thick dashed curves, $\kappa = 0.226$ the thin dashed curves, $\kappa = \frac{1}{2}$ the dotted curves separately for the mean fibre angles $\varphi = 30°, 45°$ and $60°$, and $\kappa = \frac{1}{3}$ is the solid curves. Figure (b) is a zoom of (a) for small values of the pressure.

equations (4.11) and (2.32), gives

$$\lambda\hat{\psi}_\lambda = c(\lambda^2 - \lambda^{-2}\lambda_z^{-2}) + 2k_1 \exp[k_2(I_4^* - 1)^2](I_4^* - 1)\lambda\frac{\partial I_4^*}{\partial\lambda}, \tag{4.12}$$

with

$$\lambda\frac{\partial I_4^*}{\partial\lambda} = 2[\kappa(\lambda^2 - \lambda^{-2}\lambda_z^{-2}) + (1 - 3\kappa)\lambda^2\cos^2\varphi]. \tag{4.13}$$

As noted in §2*c*, $\lambda^2\lambda_z - 1$ has the same sign at every point of the wall thickness. Thus, since the neo-Hookean shear modulus c is positive the contribution of the neo-Hookean term to equation (4.12) is positive during inflation provided $\lambda^2\lambda_z - 1 > 0$ ($=0$ in the reference configuration). For $\lambda_z = 1$ this is clearly the case since increasing radius corresponds to $\lambda > 1$. Also $k_1 > 0$ and the exponential is positive. Thus, we examine the signs of $I_4^* - 1$ and $\partial I_4^*/\partial\lambda$.

First, for $0 \le \kappa \le \frac{1}{3}$ we have $\partial I_4^*/\partial\lambda \ge 0$ and we have already noted that $I_4^* - 1 \ge 0$. Now consider $\frac{1}{3} < \kappa \le \frac{1}{2}$. For illustration we take $\kappa = \frac{1}{2}$ and $\lambda_z = 1$. Then, with $\lambda > 1$ we obtain

$$I_4^* - 1 = \frac{1}{2}\lambda^{-2}(\lambda^2 - 1)(\lambda^2 \sin^2\varphi - 1) \quad \text{and} \quad \lambda\frac{\partial I_4^*}{\partial\lambda} = \lambda^{-2}(\lambda^4 \sin^2\varphi - 1), \tag{4.14}$$

so that $I_4^* - 1 < 0$ for $\lambda < 1/\sin\varphi$ and $\partial I_4^*/\partial\lambda < 0$ for $\lambda^2 < 1/\sin\varphi$. Thus the exponential term in (4.12) is negative for

$$\frac{1}{\sqrt{\sin\varphi}} < \lambda < \frac{1}{\sin\varphi}. \tag{4.15}$$

As inflation proceeds from $\lambda = 1$ there will be parts of the integrand that are negative and this is sufficient to generate not only a maximum in P followed by a minimum but also a negative value of P, which is physically unrealistic. This is even more apparent in the membrane approximation since the pressure is then proportional to the expression in equation (4.12), which is negative for λ satisfying equation (4.15).

The study by Freed (2008) also discussed an equivalent of the structure tensor (4.5) for the three-dimensional case. The latter was used in the analysis of some simple modes of deformation by Freed (2009). Similar 'structure-like' tensors were also discussed by Federico & Herzog (2008*a*) in describing anisotropy of permeability in porous media. In addition, the model (4.11) was also used to capture the mechanical properties of pulmonary alveoli, which consist of collagen of types I and III, elastin and proteoglycans (Wiechert *et al.* 2009). In a recent paper by Haskett *et al.* (in press) the model was also used to fit data on abdominal aortas in order to evaluate the change in stiffness and anisotropy with age. A variant of the model that uses a (discretized) Gaussian distribution for the fibre orientation concentration has been used to model human aortic valve leaflets (Driessen *et al.* 2007, 2008; Balguid *et al.* 2008).

The recent study by Cortes *et al.* (in press) uses the formulation based on the generalized structure tensor (4.3) for quantitative comparisons with an angular integration formulation in which the strain energy and stresses are calculated by integrating the energy and stresses of the individual fibres, as in, for example, connective tissues (Lanir 1983), aortic valve cusps (Billiar & Sacks 2000), corneal stroma (Nguyen *et al.* 2008), articular cartilage (Ateshian *et al.* 2009) or the posterior sclera (Girard *et al.* 2009). Cortes *et al.* (in press) derived analytically the differences between the general structure tensor and angular integration formulations. On the basis of the strain-energy function (2.22) and the von Mises distribution in the form (4.8) they also illustrated numerical comparisons for three loading configurations, specifically uniaxial tension, (equi)biaxial tension

and simple shear, vis-à-vis the angular distribution. In particular, they found that for equibiaxial deformation and planar distributions the two formulations give equivalent results.

However, it should be mentioned that Cortes *et al.* (in press) assert, following Federico & Herzog (2008*b*), that the structure tensor approach is limited to situations in which the fibres are in tension and the angular distribution of the fibres is small. However, this assertion is unfounded and is based on a misinterpretation of the discussion of the generalized structure tensor introduced in Gasser *et al.* (2006). In the last paper it was stated that in a fibre distribution the anisotropic part of the structure tensor contributes to the strain energy only if the *mean* fibre direction is extended. It was not required that all fibres in the distribution be extended or be under tension. This distinguishes a fibre distribution from the situation in which fibres are aligned. Indeed, the mechanics of fibres within a distribution are quite subtle, and it is appropriate to illustrate this briefly with a simple example.

Consider a homogeneous material with a transversely isotropic distribution of fibres and mean fibre direction $\mathbf{M}$ in the reference configuration. Suppose that the material is subject to a homogeneous deformation corresponding to simple tension $\sigma > 0$ in the direction $\mathbf{M}$, so that the Cauchy stress tensor is $\boldsymbol{\sigma} = \sigma \mathbf{M} \otimes \mathbf{M}$. Let λ be the stretch in the direction $\mathbf{M}$. Then, by symmetry and incompressibility, the two transverse stretches are equal to $\lambda^{-1/2}$. Now consider a fibre within the distribution whose direction in the reference configuration, $\mathbf{A}$ say, makes an angle α with the mean direction, so that $\mathbf{A} \cdot \mathbf{M} = \cos\alpha$. Then, the stretch λ_a in the direction of this particular fibre is given by $\lambda_a^2 = \lambda^2 \cos^2\alpha + \lambda^{-1} \sin^2\alpha$. This fibre is stretched under the deformation if $\lambda_a > 1$. For $\lambda > 1$, after removal of a factor $\lambda - 1$, this inequality can be written as $\tan^2\alpha < \lambda(\lambda + 1)$. Thus, all fibres whose initial direction is such that $\tan\alpha < \sqrt{2}$ are stretched during the deformation. This gives a value of α of about 55°, which cannot be considered as 'small'. Of course, for other deformations, fibres within a distribution may be stretched only for smaller angular distributions. But this is not the real issue since we do not require all fibres in a distribution to be stretched. A telling point is that for this simple tension problem the stress along the considered fibre is $(\boldsymbol{\sigma}\mathbf{a}) \cdot \mathbf{a}$, where $\mathbf{a}$ is a unit vector in the deformed fibre direction and $\lambda_a \mathbf{a}$ is the 'push forward' of $\mathbf{A}$ under the deformation, so that the component of $\mathbf{a}$ in the direction $\mathbf{M}$ is $\lambda \cos\alpha/\lambda_a$. This results in the fibre stress $\sigma\lambda^2 \cos^2\alpha/\lambda_a^2$, which is non-negative for all α. Thus, for the considered deformation, all fibres in the distribution are under tension. But, as shown above, fibres for which α is greater than $\tan^{-1}\sqrt{2}$ are nevertheless subject to contraction initially as λ increases from 1.

An interesting application of the dispersion model is to the human cornea, for which it was found to be important to account for the dispersed collagen fibrillar structure (Pandolfi & Holzapfel 2008). This was modelled using two families of dispersed fibrils with the strain-energy function

$$\Psi(I_1, I_4^*, I_6^*) = \frac{c}{2}(I_1 - 3) + \sum_{i=4,6} \frac{k_1}{2k_2}\{\exp[k_2(I_i^* - 1)^2] - 1\}, \tag{4.16}$$

where, similarly to I_4^*, I_6^* is defined as $\kappa I_1 + (1 - 3\kappa) I_6$. Figure 13 shows the influence of the dispersion parameter κ on the mechanical response of a cornea at an intraocular (physiological) pressure of 16 mm Hg. 'Baseline' refers to a

reference simulation using two families of collagen fibrils considering dispersion according to equation (4.16), 'isotropic' uses the neo-Hookean model ($\kappa = \frac{1}{3}$), 'fibres' refers to the case $\kappa = 0$ and 'mixed' uses the baseline distribution along the superior–inferior meridian (north–south direction) and $\kappa = 0$ along the nasal–temporal meridian (west–east direction). As can be seen the stress patterns change considerably with the assumptions made regarding the degree of fibril dispersion.

(ii) *The case of a planar fibre distribution*

For thin lamellar tissue structures, which may be treated on the basis of membrane or thin shell theory, it is appropriate to consider a planar distribution of fibres within the membrane. Then, in this two-dimensional situation we consider a distribution with the fibre direction

$$\mathbf{M} = \cos\Theta\,\mathbf{e}_1 + \sin\Theta\,\mathbf{e}_2, \tag{4.17}$$

as indicated in figure 14, for Θ between $-\pi/2$ and $+\pi/2$, where $\mathbf{e}_1$ and $\mathbf{e}_2$ are rectangular Cartesian basis vectors. The counterpart of the three-dimensional structure tensor defined in equation (4.3) has in general three (in-plane) components, but for a fibre distribution that is symmetrical about the $\mathbf{e}_1$ direction the orientation density function satisfies $\rho(-\Theta) = \rho(\Theta)$, the mean fibre direction is $\mathbf{e}_1$ and only one independent component remains, as in the three-dimensional situation. The normalization condition can be written as

$$\frac{1}{\pi}\int_{-\pi/2}^{\pi/2} \rho(\Theta)\,\mathrm{d}\Theta = 1, \tag{4.18}$$

and the two-dimensional structure tensor is now defined by

$$\mathbf{H} = \frac{1}{\pi}\int_{-\pi/2}^{\pi/2} \rho\mathbf{M}\otimes\mathbf{M}\,\mathrm{d}\Theta = \kappa\mathbf{I} + (1-2\kappa)\mathbf{e}_1\otimes\mathbf{e}_1, \tag{4.19}$$

where $\mathbf{I}$ is here the two-dimensional identity and

$$\kappa = \frac{1}{\pi}\int_{-\pi/2}^{\pi/2} \rho(\Theta)\sin^2\Theta\,\mathrm{d}\Theta. \tag{4.20}$$

Now, for $\kappa = 0$ all the fibres are in the $\mathbf{e}_1$ direction, i.e. there is no dispersion, while for $\kappa = \frac{1}{2}$ the fibres are uniformly distributed in all in-plane directions (planar isotropy).

Finally in this section we note that the analogue of equation (4.6) for two dimensions is

$$I_4^* = \kappa I_1 + (1-2\kappa)I_4, \tag{4.21}$$

where $I_4 = \mathbf{e}_1\cdot(\mathbf{C}\mathbf{e}_1)$. This two-dimensional case was discussed in Ogden (2009) and an equivalent form was derived by Freed (2008, eqn 21). The relation $(4.19)_2$ was also mentioned in the recent work by Cortes *et al.* (in press).

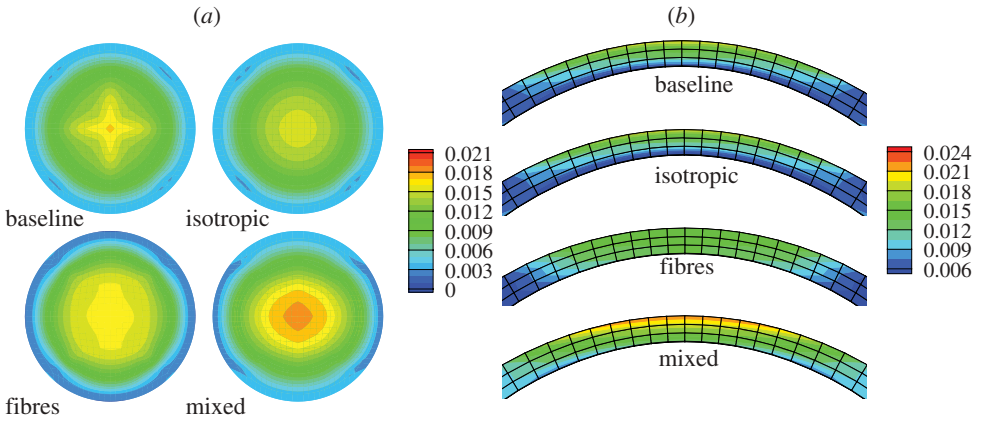

Figure 13. Stress distribution in a cornea at an intraocular pressure of 16 mm Hg using four different constitutive models (described in the text). (*a*) von Mises stress. (*b*) Maximum principal Cauchy stress. Stresses are given in MPa. Adapted from Pandolfi & Holzapfel (2008).

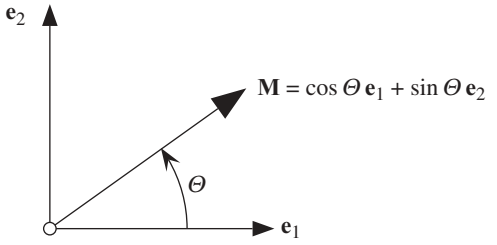

Figure 14. Characterization of an arbitrary unit direction vector $\mathbf{M}$ by means of the angle $\Theta \in [-\pi/2, +\pi/2]$ in a two-dimensional Cartesian coordinate system $\{\mathbf{e}_1, \mathbf{e}_2\}$.

5. Active response of artery walls

The models discussed so far have all been based on the passive behaviour, i.e. without consideration of the activation of smooth muscle cells. Relatively little work has been done on the modelling of activation in the continuum context. Smooth muscle cells, which are contained in the middle layer of an artery, are important constituents of the vascular system and they are responsible for control of short-term changes in lumen diameter and of long-term changes in the extracellular matrix turnover (e.g. Li *et al.* 1998).

In this section we provide an overview of the relevant continuum modelling aspects. First, however, we briefly refer to the history of the theory of muscle activation, which dates back to the work of Hill (1938). Based on the three-element Hill model several models have been developed; here, however, we mention in particular the papers by Ettema & Meijer (2000), Lloyd & Besier (2003) and Lichtwark & Wilson (2005), which collectively provide an overview of the literature although they do not particularly focus on the contraction of smooth muscle cells. Papers which capture smooth muscle contractions and related models, also based on the Hill model, are those by Gestrelius & Borgström (1986), Yang *et al.* (2003*a*) and Zulliger *et al.* (2004*b*), which are now summarized briefly.

Gestrelius & Borgström (1986) proposed a one-dimensional dynamic model of smooth muscle contraction. The model describes the energy transfer via cross-bridges and takes account of experimental observations that could not be captured by the classical Hill model. Yang *et al.* (2003*a*) presented an integrated electrochemical and mechanochemical model of the smooth muscle cell. The mechanochemical component, in particular, couples the model of Hai & Murphy (1988) with a mechanical model based on that of Hill. The mechanical model is similar to that of Gestrelius & Borgström (1986) but is extended to incorporate viscoelasticity.

A different approach to modelling the vascular smooth muscle tone was proposed by Zulliger *et al.* (2004*b*). Their phenomenological model is based on three-dimensional continuum mechanics and uses a pseudo-strain-energy function that incorporates parameters describing the mechanical properties. The pseudo-strain energy is decomposed into the sum of contributions from collagen, elastin and vascular smooth muscle. The model captures the interaction between mechanical stretch and myogenic contraction and was used in particular to illustrate localized reduction of the circumferential stress in an arterial wall due to vascular smooth muscle tone. This follows the earlier work of Rachev & Hayashi (1999) in which a simpler phenomenological model was developed based on an elastic strain-energy function and a proposed model for the active circumferential stress. In particular, the results of this work show that incorporation of the basal muscular tone into the model reduces the computed stress gradients in the wall beyond the reduction due to residual stress, which is consistent with experimental findings documented by Matsumoto & Hayashi (1996). The active response is assumed to be controlled by the concentration of free intracellular calcium (Ca^{2+}) together with the muscle fibre stretch, $\bar{\lambda}$ say, relative to a reference sarcomere length. The active stress $\boldsymbol{\sigma}_{\mathrm{a}}$ may therefore be given in the form

$$\boldsymbol{\sigma}_{\mathrm{a}} = A(\mathrm{Ca}^{2+})\bar{\lambda}\left[1 - \left(\frac{\lambda_{\mathrm{m}} - \bar{\lambda}}{\lambda_{\mathrm{m}} - \lambda_0}\right)^2\right]\mathbf{m}\otimes\mathbf{m}, \tag{5.1}$$

where $\mathbf{m}$ is a unit vector in the direction of the deformed muscle fibre, A is an activation function, λ_{m} and λ_0 are stretches at which the active force generated is a maximum and a minimum, respectively. In Rachev & Hayashi (1999) the passive state was described by $A = 0$, the basal state by $A \approx 50\,\mathrm{kPa}$ and the fully activated state by $A \approx 100\,\mathrm{kPa}$. The same activation was used in the study by Baek *et al.* (2007*a*) in conjunction with a constitutive law of the type (2.29). They developed a theory of small deformations superimposed on a large deformation in the context of fluid–solid interactions, and they showed that the theory predicts that the stiffness of the wall decreases with increasing vasoconstriction.

The more recent paper by Stålhand *et al.* (2008) uses an explicit connection between the calcium ion level and the active stress–stretch response in a one-dimensional model. The thermodynamically consistent model uses the chemical state law of Hai & Murphy (1988) and a model for smooth muscle contraction that reduces to the model of Yang *et al.* (2003*a*,*b*) in the linear limit of small deformations. It appears that the approach of Stålhand *et al.* (2008) is the first to use a strain-energy function involving the chemical kinetics of smooth muscle

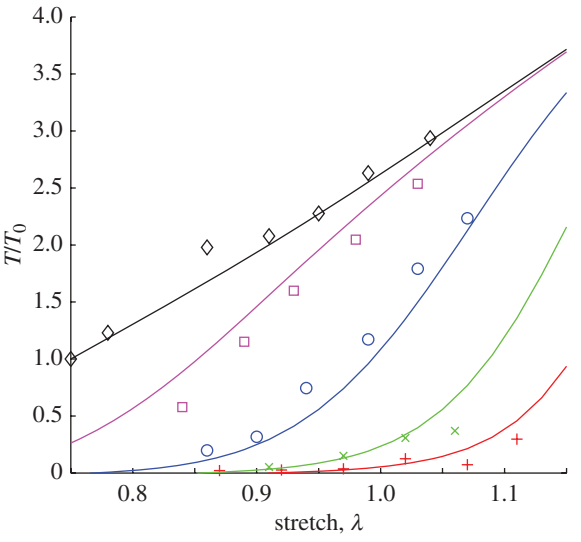

Figure 15. Stress versus stretch as a function of the calcium ion concentration given in micromoles per litre (μM). The stress is normalized with respect to the minimum stress in the maximally activated state, denoted by T_0. Data are taken from Hunter *et al.* (1998); solid curves represent results from the model. Reprinted from Stålhand *et al.* (2008) with permission from Elsevier. Red curve and red plus symbol, $[\mathrm{Ca}]^{2+} = 1.9\,\mu\mathrm{M}$; green curve and green cross symbol, $[\mathrm{Ca}]^{2+} = 2.7\,\mu\mathrm{M}$; blue curve and blue open circle, $[\mathrm{Ca}]^{2+} = 4.3\,\mu\mathrm{M}$; pink curve and pink square, $[\mathrm{Ca}]^{2+} = 8.9\,\mu\mathrm{M}$; black curve and black open diamond, $[\mathrm{Ca}]^{2+} > 10\,\mu\mathrm{M}$.

contraction and nonlinear kinematics. This approach can easily be extended to other constitutive models, including three-dimensional models, and facilitates implementation in finite element codes. Figure 15 shows the dependence of the active stress ratio T/T_0 on the stretch λ in terms of the calcium ion concentration Ca^{2+}, where T_0 is the minimum stress in the maximally activated state. The experimental data are taken from Hunter *et al.* (1998). For maximally activated muscles, the stress is a linear function of the stretch, unlike the situation for lower activation levels.

A thermodynamically consistent mechanochemical model for the prediction of force generation in smooth muscle was proposed recently by Murtada *et al.* (in press). It is a simple model incorporating only a few material parameters, each of which has a clear physical meaning. In this model the strain-energy function is expressed in the form

$$\varPsi = \varPsi_{\mathrm{p}} + \varPsi_{\mathrm{a}}, \tag{5.2}$$

where $\varPsi_{\mathrm{p}}$ describes the passive elastic response and $\varPsi_{\mathrm{a}}$ describes the active response, which is the energy stored in the network of contractile units. Specifically, $\varPsi_{\mathrm{p}}$ was taken to be the neo-Hookean model but could be replaced by a more general elastic model such as that in equation (2.29), while $\varPsi_{\mathrm{a}}$ was used in the form

$$\varPsi_{\mathrm{a}} = \frac{\mu_{\mathrm{a}}}{2}\,(n_{\mathrm{C}} + n_{\mathrm{D}})\,(\lambda_{\mathrm{f}} + \bar{u}_{\mathrm{rs}} - 1)^2, \tag{5.3}$$

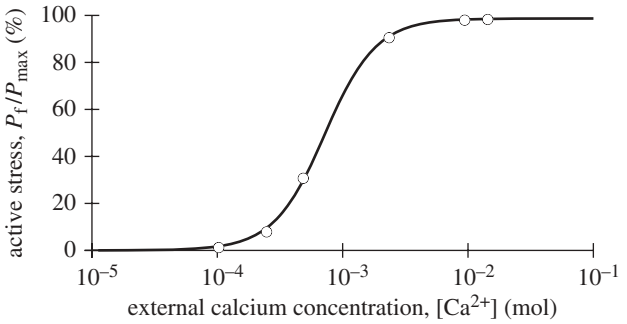

Figure 16. Relationship between the active stress in per cent of the maximum active stress and the external calcium concentration $[Ca^{2+}]$. Solid black line, model; open circle, experimental data (Arner 1982).

where μ_a is a parameter related to activation, n_C and n_D are fractional concentrations of the force-generating states C and D, which correspond to myosin heads attached or unattached, respectively, to the actin filaments (see the model of Hai & Murphy 1988), λ_f is the stretch of the contractile unit and $\bar{u}_{rs}$ is the normalized relative sliding displacement between the myosin and actin filaments. The internal state variable $\bar{u}_{rs}$ is governed by an evolution equation, details of which can be found in Murtada *et al.* (in press). The results of the coupled mechanochemical model are consistent with isometric and isotonic experiments on smooth muscle tissue. For example, figure 16 shows the relationship between the active stress (P_f/P_{max}) as a percentage of the maximum active stress versus the external calcium concentration $[Ca^{2+}]$ based on the model and data from the paper by Arner (1982), which involved activation of intact smooth muscle tissues with different external calcium concentrations. The correlation with the data is excellent.

The aforementioned model was extended by Murtada *et al.* (submitted) to account for the dispersion in the orientation of contractile fibres in smooth muscles so as to capture available experimental data. Therein it is shown that the orientation of smooth muscle myofilaments has a strong influence on the contraction response.

6. Conclusions and future directions

It is well known that arteries are subject to finite deformations and that their mechanical behaviour is highly nonlinear, anisotropic and essentially incompressible in the physiological domain.

It is also the case that the mechanical response can be regarded as purely elastic in many circumstances and that the constitutive properties of artery wall tissue can be characterized in terms of strain-energy functions. There is now a well-established theoretical framework for treating the elastic behaviour of arteries on the basis of deformation invariants that reflect aspects of the structure of arteries, in particular the directions distinguished by the collagen fibre structure, in which sense the framework can be regarded as structural, or

at least structurally motivated. The present review article has focused on the development of constitutive laws constructed within this framework and it is therefore limited by the geometrical assumptions embodied by the framework and hence modest in its objectives.

Nevertheless, it provides an overview, covering essentially the last 10 years, of the state of the art in the constitutive modelling of the passive response of arteries together with a brief account of the much less well-developed modelling of the active response. The structure of soft tissues is, of course, far more complex than is suggested by the relatively simple model based on collagen fibres embedded in an isotropic matrix of ground substance, and much remains to be done in terms of modelling.

The increasing effort devoted to studies of mechanical models for the cardiovascular system and their applications aimed at refining basic and clinical analyses demonstrates the vitality of the field of biomechanics. Some future directions on which research on arteries might focus are discussed below.

In this regard we have the excellent review by Humphrey (2003) to guide our hand. This covers many aspects of the biomechanics of soft tissues, including artery wall tissue, and identifies open problems that call for a multi-disciplinary approach involving applied mechanics, biomechanics, mathematics and mechanobiology. The needs he identifies are embraced by the sentence 'Because of the inherent complexities of the microstructure and biomechanical behaviour of biological cells and tissues, there is a need for new theoretical frameworks to guide the design and interpretation of new classes of experiments'.

Whilst Humphrey's review covers a wide range of soft tissues, that of Humphrey & Taylor (2008) is more specific in that it compares and contrasts the biology and mechanics of intracranial and abdominal aortic aneurysms. They emphasize the need to couple more effectively the wall biosolid mechanics with the biofluid dynamics of blood flow, vascular biology and medical imaging in order to improve understanding of the mechanobiology and pathophysiology of aneurysms and their treatment. The very recent review by Taylor & Humphrey (2009) has a more general focus on the role of computational approaches within vascular biomechanics and also emphasizes the need for multi-disciplinary research towards improving understanding of vascular physiology and pathology along with improving the design of medical devices and clinical interventions. Throughout these reviews the important roles and further potential of nonlinear continuum biomechanics and computational mechanics are emphasized.

The study of the biomechanics of artery walls and other soft tissues is really in its infancy and there is much more research needed in order to gain understanding of the interactions between the constituents within the complex structure and their influence on the mechanical and mechanobiological behaviour in both healthy and diseased tissue. Here we highlight a few key issues that deserve to attract much research effort over the next few years. Our discussion is confined to artery wall mechanics, although many issues can be considered more broadly applicable to soft tissues.

First, at the macroscopic level, the development of constitutive laws that model the (three dimensional) active response of arteries is very important since contraction of the smooth muscle cells within the wall can change significantly the artery cross section and thereby regulate blood flow. It is

therefore essential to couple the mechanics with the biochemistry by focusing on the structure of the contractile units, but it is also important to incorporate in the constitutive law only a few material parameters, each of which has a clear physical meaning. The consistency of the model then needs to be demonstrated by comparison with experimental data obtained from activating smooth muscle cells.

In order to better understand the changes of the artery cross section due to smooth muscle activation there is also a need to consider in more detail the coupling of arterial wall mechanics and haemodynamics, i.e. fluid–solid interactions. This inevitably requires a computational mechanics approach, as argued so eloquently by Taylor & Humphrey (2009). In this respect computational methods such as finite element methods have a key role to play in order to provide more realistic simulations of clinical interventions and patient-specific geometric modelling, which should also take account of the influence of the surrounding (perivascular) tissue with appropriate boundary conditions. This requires more information about the evolution of *in vivo* material properties and a better understanding of the *in vivo* conditions. Computational biomechanics, now a well-defined field in its own right, is increasing our ability to address multi-disciplinary problems of academic, industrial and clinical importance. In particular, it is bridging the gap between the different length scales and between basic research and clinical application, thereby aiding the transfer of biomechanics from the laboratory bench to the bedside. Computational models, when based on appropriate three-dimensional constitutive laws, have the potential to realistically predict physiological functional interactions, to better repair injuries, to improve diagnostics, treatment of disease, surgical planning and intervention, and to improve the success of implanted prostheses, whether manufactured or tissue engineered. Computational methods will increasingly assist the development of refined models by, for example, incorporating spatial variations of tissue properties. As with any simulation, computational biomechanical models need to prove both their accuracy and their worth, i.e. numerical results need to correlate well with experimental data at the tissue, cellular and molecular levels. For a review of the application of computational mechanics to the diagnosis and treatment of cardiovascular disease, see del Álamo *et al.* (2009). A more specific review of computational modelling involving fluid–structure interactions in vascular anastomoses is provided by Migliavacca & Dubini (2005).

More refinements in the modelling are needed at the structural level, taking us beyond the influence of collagen fibre orientation to include the separate properties and contributions of other key constituents, such as elastin and smooth muscle, and their mutual interactions, to build more comprehensive mechanical models. Much more data are needed to inform the modelling, in particular stress–strain data from multi-axial tests. Ultimately, the behaviour of tissues derives from their constituents at the mesoscopic level, which in turn derive from the aggregate of the molecules that form them. Thus, knowledge of the biomechanical properties of individual molecules will be an important ingredient in building multi-scale models from the microscopic to the mesoscopic to the macroscopic level. For example, drug therapy or biocompatible body part replacement depends on knowing how proteins and cells behave in context and in their interaction with surrounding tissues so as to generate function at a

higher level. Hence multi-scale approaches provide ongoing challenges in vascular biomechanics, where simulation and experiment must go hand-in-hand to achieve this integrative knowledge.

The above considerations apply in the first instance to healthy tissue, and provide a starting point for understanding the biomechanics and mechanobiology of tissues in general, both healthy and diseased. Biomechanics and mechanobiology have particularly important contributions to make to the understanding of changes in the vascular system associated with ageing and disease. Associated with ageing there is, in particular, a degradation of elastin and consequent loss of arterial elasticity, an increase in collagen density and hence stiffness of the artery (decreased distensibility), and reduction in smooth muscle contractility. Elastin degradation that links to, for example, deviations of wall shear stresses from normotensive levels, remodelling of collagen that maintains an equilibrium level of strain, and reduction of smooth muscle cell contraction is also a feature in the development of aneurysms. There is therefore a need to better understand these changes by using suitable constitutive models, patient-specific arterial geometries and a link of the chemomechanics of arterial growth and remodelling to mechanical stimuli resulting from circulatory pressure and flow. Research in this direction will provide the basis for further elucidating the aetiology of aneurysmal disease. In hypertension arteries increase (or decrease) their wall thickness in response to sustained increases (or decreases) in blood pressure, and there is also an important effect associated with changes in blood flow-induced wall shear stress—the lumen diameter increases (decreases) with sustained increases (decreases) in wall shear stress. In addition, shear stresses affect plaque composition and induce atherogenesis, and low and oscillatory shear stresses induce atherosclerotic plaques. This once again brings to the fore the need to better understand the coupling of the wall solid mechanics with the blood fluid dynamics.

Other (pathological) changes in the artery wall are associated with atherosclerosis, commonly referred to as ‘hardening of the arteries’, which is a widespread vascular disease caused by thickening of the intima due to deposition of, for example, fatty substances, collagen fibres and cellular waste products (collectively called plaque). These pathological changes are associated with significant alterations in the material properties of the arterial wall. In order to access the heterogeneous morphologies of such plaques specific imaging modalities are required. The combination of image analysis, biomechanics and mechanobiology provides then an efficient basis for a thorough patient-specific study of the relationship between morphological, structural and (in)elastic constitutive data under various loading conditions. There is some evidence that such computational approaches, when based on *in vivo* imaging, can provide reliable answers to clinical questions raised by, for example, cardiologists and will play a larger role in cardiovascular research and medicine in the near future.

A general feature of all these changes is that the material properties and geometry evolve in time, and to understand these diseases in more detail it is important to be able to model this evolving histology and mechanobiology, which involves growth, remodelling and adaptation. The modelling of growth and remodelling is receiving much attention in the literature, but it is fair to say that the theory is as yet not well established and the underlying mechanisms are not well understood, so there is much to be learned about the processes

involved, such as the changing material properties and the turnover, production and removal of constituents. Changes that occur in adaptation to changes in the mechanical environment associated with damage and repair will also require similar modelling approaches.

In addition, there is a need to understand the influence of growth and remodelling on the development of residual stresses and to incorporate residual stresses within the constitutive modelling framework. In particular, it is emphasized that quantitative data on residual stresses are difficult to obtain so that new methods are required for gathering such data, which are needed to inform the modelling process.

In fact, it is not generally clear what the origin of residual stresses is, and this therefore requires further investigation. One suggestion of a possible factor is contained in the recent study by Azeloglu *et al.* (2008), in which it is hypothesized that the transmural distribution of the fixed charged density of the proteoglycans has a significant role in regulating residual stresses.

This hypothesis was tested theoretically and implemented in a finite element model and it was confirmed that the hypothetical mechanism yielded opening angles in the range reported in the literature.

Based on a constrained mixture model the influence of elastin, collagen and smooth muscle cell contributions to residual stresses of artery walls has been analysed in a recent theoretical paper by Cardamone *et al.* (2009), while an initial analysis of three-dimensional residual stresses in a layered artery was recently documented by Holzapfel & Ogden (2010).

These recent contributions form important steps towards an integrated understanding of the biomechanics and mechanobiology of residual stresses.

Financial support for this research was partly provided through an International Joint Project grant from the Royal Society of London. This support is gratefully acknowledged.

References

Alastrué, V., Calvo, B., Peña, E. & Doblaré, M. 2006 Biomechanical modeling of refractive corneal surgery. *J. Biomech. Eng.* **128**, 150–160. (doi:10.1115/1.2132368)

Alastrué, V., Martínez, M. A. & Doblaré, M. 2008*a* Modelling adaptative volumetric finite growth in patient-specific residually stressed arteries. *J. Biomech.* **41**, 1773–1781. (doi:10.1016/j.jbiomech.2008.02.036)

Alastrué, V., Peña, E., Martínez, M. A. & Doblaré, M. 2008*b* Experimental study and constitutive modelling of the passive mechanical properties of the ovine infrarenal vena cava tissue. *J. Biomech.* **41**, 3038–3045. (doi:10.1016/j.jbiomech.2008.07.008)

Alford, P. W., Humphrey, J. D. & Taber, L. A. 2008 Growth and remodeling in a thick-walled artery model: effects of spatial variations in wall constituents. *Biomech. Model. Mechanobiol.* **7**, 245–262. (doi:10.1007/s10237-007-0101-2)

Arner, A. 1982 Mechanical characteristics of chemically skinned guinea-pig taenia coli. *Eur. J. Physiol.* **395**, 277–284. (doi:10.1007/BF00580790)

Ateshian, G. A., Rajan, V., Chahine, N. O., Canal, C. E. & Hung, C. T. 2009 Modeling the matrix of articular cartilage using a continuous fiber angular distribution predicts many observed phenomena. *J. Biomech. Eng.* **131**, 061003. (doi:10.1115/1.3118773)

Azeloglu, E. U., Albro, M. B., Thimmappa, V. A., Ateshian, G. A. & Costa, K. D. 2008 Heterogeneous transmural proteoglycan distribution provides a mechanism for regulating residual stresses in the aorta. *Am. J. Physiol. Heart Circ. Physiol.* **294**, H1197–H1205. (doi:10.1152/ajpheart.01027.2007)

Baek, S., Gleason, R. L., Rajagopal, K. R. & Humphrey, J. D. 2007*a* Theory of small on large: potential utility in computations of fluid–solid interactions in arteries. *Comput. Meth. Appl. Mech. Eng.* **196**, 3070–3078. (doi:10.1016/j.cma.2006.06.018)

Baek, S., Valentín, A. & Humphrey, J. D. 2007*b* Biochemomechanics of cerebral vasospasm and its resolution. II. Constitutive relations and model simulations. *Ann. Biomed. Eng.* **35**, 1498–1509. (doi:10.1007/s10439-007-9322-x)

Balguid, A., Driessen, N. J., Mol, A., Schmitz, J. P., Verheyen, F., Bouten, C. V. & Baaijens, F. P. 2008 Stress related collagen ultrastructure in human aortic valves—implications for tissue engineering. *J. Biomech.* **41**, 2612–2617. (doi:10.1016/j.jbiomech.2008.06.031)

Balzani, D., Neff, P., Schröder, J. & Holzapfel, G. A. 2006 A polyconvex framework for soft biological tissues. Adjustment to experimental data. *Int. J. Solids Struct.* **43**, 6052–6070. (doi:10.1016/j.ijsolstr.2005.07.048)

Billiar, K. L. & Sacks, M. S. 2000 Biaxial mechanical properties of fresh and glutaraldehyde treated porcine aortic valve cusps. Part II. A structurally guided constitutive model. *J. Biomech. Eng.* **122**, 327–335. (doi:10.1115/1.1287158)

Cacho, F., Doblaré, M. & Holzapfel, G. A. 2007 A procedure to simulate coronary artery bypass graft surgery. *Med. Biol. Eng. Comput.* **45**, 819–827. (doi:10.1007/s11517-007-0201-2)

Cardamone, L., Valentín, A., Eberth, J. F. & Humphrey, J. D. 2009 Origin of axial prestretch and residual stress in arteries. *Biomech. Model. Mechanobiol.* **8**, 431–446. (doi:10.1007/s10237-008-0146-x)

Carew, T. E., Vaishnav, R. N. & Patel, D. J. 1968 Compressibility of the arterial wall. *Circ. Res.* **23**, 61–68.

Chen, H. Y., Navia, J. A. & Kassab, G. A. 2009 A simulation of vessel-clamp interaction: transient closure dynamics. *Ann. Biomed. Eng.* **37**, 1772–1780. (doi:10.1007/s10439-009-9748-4)

Ciarletta, P., Dario, P., Tendick, F. & Micera, S. 2009 Hyperelastic model of anisotropic fiber reinforcements within intestinal walls for applications in medical robotics. *Int. J. Robot. Res.* **28**, 1279–1288. (doi:10.1177/0278364909101190)

Cortes, D. H., Lake, S. P., Kadlowec, J. A., Soslowsky, L. J. & Elliott, D. M. In press. Characterizing the mechanical contribution of fiber angular distribution in connective tissue: comparison of two modeling approaches. *Biomech. Model. Mechanobiol.* (doi:10.1007/s10237-010-0194-x)

del Álamo, J. C., Marsden, A. L. & Lasheras, J. C. 2009 Recent advances in the application of computational mechanics to the diagnosis and treatment of cardiovascular disease. *Rev. Esp. Cardiol.* **62**, 781–805.

Dokos, S., Smaill, B. H., Young, A. A. & LeGrice, I. J. 2002 Shear properties of passive ventricular myocardium. *Am. J. Physiol.* **283**, H2650–H2659.

Driessen, N. J., Mol, A., Bouten, C. V. & Baaijens, F. P. 2007 Modeling the mechanics of tissue-engineered human heart valve leaflets. *J. Biomech.* **40**, 325–334. (doi:10.1016/j.jbiomech.2006.01.009)

Driessen, N. J., Cox, M. A., Bouten, C. V. & Baaijens, F. P. 2008 Remodelling of the angular collagen fiber distribution in cardiovascular tissues. *Biomech. Model. Mechanobiol.* **7**, 93–103. (doi:10.1007/s10237-007-0078-x)

Eberlein, R., Holzapfel, G. A. & Schulze-Bauer, C. A. J. 2001 An anisotropic model for annulus tissue and enhanced finite element analyses of intact lumbar disc bodies. *Comput. Meth. Biomech. Biomed. Eng.* **4**, 209–230. (doi:10.1080/10255840108908005)

Eberlein, R., Holzapfel, G. A. & Fröhlich, M. 2004 Multi-segment FEA of the human lumbar spine including the heterogeneity of the annulus fibrosus. *Comput. Mech.* **34**, 147–163. (doi:10.1007/s00466-004-0563-3)

Eriksson, T., Kroon, M. & Holzapfel, G. A. 2009 Influence of medial collagen organization and axial *in situ* stretch on saccular cerebral aneurysm growth. *J. Biomech. Eng.* **131**, 101010. (doi:10.1115/1.3200911)

Ettema, G. J. & Meijer, K. 2000 Muscle contraction history: modified Hill versus an exponential decay model. *Biol. Cell.* **83**, 491–500.

Federico, S. & Herzog, W. 2008*a* On the permeability of fibre-reinforced porous materials. *Int. J. Solids Structures* **45**, 2160–2172. (doi:10.1016/j.ijsolstr.2007.11.014)

Federico, S. & Herzog, W. 2008*b* Towards an analytical model of soft biological tissues. *J. Biomech.* **41**, 3309–3313. (doi:10.1016/j.jbiomech.2008.05.039)

Finlay, H. M., Whittaker, P. & Canham, P. B. 1998 Collagen organization in the branching region of human brain arteries. *Stroke* **29**, 1595–1601.

Freed, A. D. 2008 Anisotropy in hypoelastic soft-tissue mechanics. I. Theory. *J. Mech. Mater. Struct.* **3**, 911–928. (doi:10.2140/jomms.2008.3.911)

Freed, A. D. 2009 Anisotropy in hypoelastic soft-tissue mechanics. II. Simple extensional experiments. *J. Mech. Mater. Struct.* **4**, 1005–1025. (doi:10.2140/jomms.2009.4.1005)

Freed, A. D., Einstein, D. R. & Vesely, I. 2005 Invariant formulation for dispersed transverse isotropy in aortic heart valves: an efficient means for modeling fiber splay. *Biomech. Model. Mechanobiol.* **4**, 100–117. (doi:10.1007/s10237-005-0069-8)

Fung, Y. C. 1967 Elasticity of soft tissues in simple elongation. *Am. J. Physiol.* **213**, 1532–1544.

Gasser, T. C. & Holzapfel, G. A. 2002 A rate-independent elastoplastic constitutive model for (biological) fiber-reinforced composites at finite strains: continuum basis, algorithmic formulation and finite element implementation. *Comput. Mech.* **29**, 340–360. (doi:10.1007/s00466-002-0347-6)

Gasser, T. C. & Holzapfel, G. A. 2006*a* 3D crack propagation in unreinforced concrete. A two-step algorithm for tracking 3D crack paths. *Comput. Meth. Appl. Mech. Eng.* **195**, 5198–5219. (doi:10.1016/j.cma.2005.10.023)

Gasser, T. C. & Holzapfel, G. A. 2006*b* Modeling the propagation of arterial dissection. *Eur. J. Mech. A Solids* **25**, 617–633. (doi:10.1016/j.euromechsol.2006.05.004)

Gasser, T. C. & Holzapfel, G. A. 2007*a* Finite element modeling of balloon angioplasty by considering overstretch of remnant non-diseased tissues in lesions. *Comput. Mech.* **40**, 47–60. (doi:10.1007/s00466-006-0081-6)

Gasser, T. C. & Holzapfel, G. A. 2007*b* Modeling plaque fissuring and dissection during balloon angioplasty intervention. *Ann. Biomed. Eng.* **35**, 711–723. (doi:10.1007/s10439-007-9258-1)

Gasser, T. C., Schulze-Bauer, C. A. J. & Holzapfel, G. A. 2002 A three-dimensional finite element model for arterial clamping. *J. Biomech. Eng.* **124**, 355–363. (doi:10.1115/1.1485284)

Gasser, T. C., Ogden, R. W. & Holzapfel, G. A. 2006 Hyperelastic modelling of arterial layers with distributed collagen fibre orientations. *J. R. Soc. Interface* **3**, 15–35. (doi:10.1098/rsif.2005.0073)

Gestrelius, S. & Borgström, P. 1986 A dynamic model of smooth muscle contraction. *Biophys. J.* **50**, 157–169. (doi:10.1016/S0006-3495(86)83448-8)

Girard, M. J., Downs, J. C., Burgoyne, C. F. & Suh J.-K. F. 2009 Peripapillary and posterior scleral mechanics. Part I. Development of an anisotropic hyperelastic constitutive model. *J. Biomech. Eng.* **131**, 051011. (doi:10.1115/1.3113682)

Gleason, R. L., Dye, W. W., Wilson, E. & Humphrey, J. D. 2008 Quantification of the mechanical behavior of carotid arteries from wild-type, dystrophin-deficient, and sarcoglycan-δ knockout mice. *J. Biomech.* **41**, 3213–3218. (doi:10.1016/j.jbiomech.2008.08.012)

Gundiah, N., Ratcliffe, M. B. & Pruitt, L. A. 2007 Determination of strain energy function for arterial elastin: experiments using histology and mechanical tests. *J. Biomech.* **40**, 586–594. (doi:10.1016/j.jbiomech.2006.02.004)

Hai, C. M. & Murphy, R. A. 1988 Cross-bridge phosphorylation and regulation of latch state in smooth muscle. *J. Appl. Physiol.* **254**, C99–106.

Hariton, I., deBotton, G., Gasser, T. C. & Holzapfel, G. A. 2007*a* Stress-driven collagen fiber remodeling in arterial walls. *Biomech. Model. Mechanobiol.* **6**, 163–175. (doi:10.1007/s10237-006-0049-7)

Hariton, I., deBotton, G., Gasser, T. C. & Holzapfel, G. A. 2007*b* Stress-modulated collagen fiber remodeling in a human carotid bifurcation. *J. Theor. Biol.* **248**, 460–470. (doi:10.1016/j.jtbi.2007.05.037)

Haskett, D., Johnson, G., Zhou, A., Utzinger, U. & Vande Geest, J. In press. Microstructural and biomechanical alterations of the human aorta as a function of age and location. *Biomech. Model. Mechanobiol.*

Hill, A. V. 1938 The heat of shortening and the dynamic constants of muscle. *Proc. R. Soc. Lond. B* **126**, 136–195. (doi:10.1098/rspb.1938.0050)

Holzapfel, G. A. 2000 *Nonlinear solid mechanics. A continuum approach for engineering.* Chichester, UK: Wiley.

Holzapfel, G. A. & Gasser, T. C. 2001 A viscoelastic model for fiber-reinforced composites at finite strains: continuum basis, computational aspects and applications. *Comput. Meth. Appl. Mech. Eng.* **190**, 4379–4403. (doi:10.1016/S0045-7825(00)00323-6)

Holzapfel, G. A. & Gasser, T. C. 2007 Computational stress–deformation analysis of arterial walls including high-pressure response. *Int. J. Cardiol.* **116**, 78–85. (doi:10.1016/j.ijcard.2006.03.033)

Holzapfel, G. A. & Ogden, R. W. (eds) 2003 *Biomechanics of soft tissue in cardiovascular systems.* Vienna, Austria: Springer-Verlag.

Holzapfel, G. A. & Ogden, R. W. (eds) 2006 *Mechanics of biological tissue.* Heidelberg: Springer-Verlag.

Holzapfel, G. A. & Ogden, R. W. (eds) 2009*a* *Biomechanical modelling at the molecular, cellular and tissue levels.* Vienna, Austria: Springer.

Holzapfel, G. A. & Ogden, R. W. 2009*b* Constitutive modelling of passive myocardium: a structurally based framework for material characterization. *Phil. Trans. R. Soc. A* **367**, 3445–3475. (doi:10.1098/rsta.2009.0091)

Holzapfel, G. A. & Ogden, R. W. 2009*c* In planar biaxial tests for anisotropic nonlinearly elastic solids. A continuum mechanical framework. *Math. Mech. Solids* **14**, 474–489. (doi:10.1177/1081286507084411)

Holzapfel, G. A. & Ogden, R. W. 2010 Modelling the layer-specific three-dimensional residual stresses in arteries, with an application to the human aorta. *J. R. Soc. Interface.* (doi:10.1098/rsif.2009.0357)

Holzapfel, G. A. & Stadler, M. 2006 Role of facet curvature for accurate vertebral facet load analysis. *Eur. Spine J.* **15**, 849–856. (doi:10.1007/s00586-004-0874-2)

Holzapfel, G. A. & Weizsäcker, H. W. 1998 Biomechanical behavior of the arterial wall and its numerical characterization. *Comput. Biol. Med.* **28**, 377–392. (doi:10.1016/S0010-4825(98)00022-5)

Holzapfel, G. A., Gasser, T. C. & Ogden, R. W. 2000*a* A new constitutive framework for arterial wall mechanics and a comparative study of material models. *J. Elasticity* **61**, 1–48. (doi:10.1023/A:1010835316564)

Holzapfel, G. A., Schulze-Bauer, C. A. J. & Stadler, M. 2000*b* Mechanics of angioplasty: wall, balloon and stent. In *Mechanics in biology* (eds J. Casey & G. Bao), pp. 141–156. New York, NY: The American Society of Mechanical Engineers (ASME), AMD-Vol. 242/BED-Vol. 46.

Holzapfel, G. A., Gasser, T. C. & Stadler, M. 2002*a* A structural model for the viscoelastic behavior of arterial walls: continuum formulation and finite element analysis. *Eur. J. Mech. A Solids* **21**, 441–463. (doi:10.1016/S0997-7538(01)01206-2)

Holzapfel, G. A., Stadler, M. & Schulze-Bauer, C. A. J. 2002*b* A layer-specific three-dimensional model for the simulation of balloon angioplasty using magnetic resonance imaging and mechanical testing. *Ann. Biomed. Eng.* **30**, 753–767. (doi:10.1114/1.1492812)

Holzapfel, G. A., Gasser, T. C. & Ogden, R. W. 2004 Comparison of a multi-layer structural model for arterial walls with a Fung-type model, and issues of material stability. *J. Biomech. Eng.* **126**, 264–275. (doi:10.1115/1.1695572)

Holzapfel, G. A., Sommer, G., Gasser, C. T. & Regitnig, P. 2005*a* Determination of the layer-specific mechanical properties of human coronary arteries with non-atherosclerotic intimal thickening, and related constitutive modelling. *Am. J. Physiol. Heart Circ. Physiol.* **289**, H2048–H2058. (doi:10.1152/ajpheart.00934.2004)

Holzapfel, G. A., Stadler, M. & Gasser, T. C. 2005*b* Changes in the mechanical environment of stenotic arteries during interaction with stents: computational assessment of parametric stent design. *J. Biomech. Eng.* **127**, 166–180. (doi:10.1115/1.1835362)

Hu, J.-J., Baek, S. & Humphrey, J. D. 2007 Stress-strain behavior of the passive basilar artery in normotension and hypertension. *J. Biomech.* **40**, 2559–2563. (doi:10.1016/j.jbiomech.2006.11.007)

Humphrey, J. D. 2002 *Cardiovascular solid mechanics. cells, tissues, and organs.* New York, NY: Springer.

Humphrey, J. D. 2003 Continuum biomechanics of soft biological tissues. *Proc. R. Soc. Lond. A* **459**, 1–44. (doi:10.1098/rspa.2002.1060)

Humphrey, J. D. & Rajagopal, K. R. 2002 A constrained mixture model for growth and remodeling of soft tissues. *Math. Model. Meth. Appl. Sci.* **12**, 407–430. (doi:10.1142/S0218202502001714)

Humphrey, J. D. & Taylor, C. A. 2008 Intracranial and abdominal aortic aneurysms: similarities, differences, and need for a new class of computational models. *Annu. Rev. Biomed. Eng.* **10**, 221–246. (doi:10.1146/annurev.bioeng.10.061807.160439)

Hunter, P. J., McCulloch, A. D. & ter Keurs, H. E. D. J. 1998 Modelling the mechanical properties of cardiac muscle. *Prog. Biophys. Mol. Biol.* **69**, 289–331. (doi:10.1016/S0079-6107(98)00013-3)

Karšaj, I., Sansour, C. & Sorić, J. 2009 The modelling of fibre reorientation in soft tissue. *Biomech. Model. Mechanobiol.* **8**, 359–370. (doi:10.1007/s10237-008-0142-1)

Kiousis, D. E., Gasser, T. C. & Holzapfel, G. A. 2007 A numerical model to study the interaction of vascular stents with human atherosclerotic lesions. *Ann. Biomed. Eng.* **35**, 1857–1869. (doi:10.1007/s10439-007-9357-z)

Kiousis, D. E., Rubinigg, S. F., Auer, M. & Holzapfel, G. A. 2009 A methodology to analyze changes in lipid core and calcification onto fibrous cap vulnerability: the human atherosclerotic carotid bifurcation as an illustratory example. *J. Biomech. Eng.* **131**, 121002.

Kroon, M. & Holzapfel, G. A. 2007 A model for saccular cerebral aneurysm growth by collagen fibre remodelling. *J. Theor. Biol.* **247**, 775–787. (doi:10.1016/j.jtbi.2007.03.009)

Kroon, M. & Holzapfel, G. A. 2008*a* Modeling of saccular aneurysm growth in a human middle cerebral artery. *J. Biomech. Eng.* **130**, 051012. (doi:10.1115/1.2965597)

Kroon, M. & Holzapfel, G. A. 2008*b* A new constitutive model for multi-layered collagenous tissues. *J. Biomech.* **41**, 2766–2771. (doi:10.1016/j.jbiomech.2008.05.033)

Kroon, M. & Holzapfel, G. A. 2009 Elastic properties of anisotropic vascular membranes examined by inverse analysis. *Comput. Meth. Appl. Mech. Eng.* **198**, 3622–3632. (doi:10.1016/j.cma.2008.08.002)

Lanchares, E., Calvo, B., Cristóbal, J. A. & Doblaré, M. 2008 Finite element simulation of arcuates for astigmatism correction. *J. Biomech.* **41**, 797–805. (doi:10.1016/j.jbiomech.2007.11.010)

Lanir, Y. 1983 Constitutive equations for fibrous connective tissues. *J. Biomech.* **16**, 1–12. (doi:10.1016/0021-9290(83)90041-6)

Länne, T., Sonesson, B., Bergqvist, D., Bengtsson, H. & Gustafsson, D. 1992 Diameter and compliance in the male human abdominal aorta: influence of age and aortic aneurysm. *Eur. J. Vasc. Surg.* **6**, 178–184. (doi:10.1016/S0950-821X(05)80237-3)

Li, D. & Robertson, A. M. 2009 A structural multi-mechanism constitutive equation for cerebral arterial tissue. *Int. J. Solids Structures* **46**, 2920–2928. (doi:10.1016/j.ijsolstr.2009.03.017)

Li, Q., Muragaki, Y., Hatamura, I., Ueno, H. & Ooshima, A. 1998 Stretch-induced collagen synthesis in cultured smooth muscle cells from rabbit aortic media and a possible involvement of angiotensin II and transforming growth factor-β. *J. Vasc. Res.* **35**, 93–103. (doi:10.1159/000025570)

Lichtwark, G. A. & Wilson, A. M. 2005 A modified Hill muscle model that predicts muscle power output and efficiency during sinusoidal length changes. *J. Exp. Biol.* **208**, 2831–2843. (doi:10.1242/jeb.01709)

Lloyd, D. G. & Besier, T. F. 2003 An EMG-driven musculoskeletal model to estimate muscle forces and knee joint moments *in vivo*. *J. Biomech.* **36**, 765–776. (doi:10.1016/S0021-9290(03)00010-1)

Lu, J., Zhou, X. & Raghavan, M. L. 2007 Computational method of inverse elastostatics for anisotropic hyperelastic solids. *Int. J. Numer. Meth. Eng.* **69**, 1239–1261. (doi:10.1002/nme.1807)

Masson, I., Boutouyrie, P., Laurent, S., Humphrey, J. D. & Zidi, M. 2008 Characterization of arterial wall mechanical behavior and stresses from human clinical data. *J. Biomech.* **41**, 2618–2627. (doi:10.1016/j.jbiomech.2008.06.022)

Matsumoto, T. & Hayashi, K. 1996 Stress and strain distribution in hypertensive and normotensive rat aorta considering residual strain. *J. Biomech.* **118**, 62–73. (doi:10.1115/1.2795947)

Merodio, J. & Ogden, R. W. 2005 Mechanical response of fiber-reinforced incompressible non-linearly elastic solids. *Int. J. Non-Linear Mech.* **40**, 213–227. (doi:10.1016/j.ijnonlinmec.2004.05.003)

Migliavacca, F. & Dubini, G. 2005 Computational modeling of vascular anastomoses. *Biomech. Model. Mechanobiol.* **3**, 235–250. (doi:10.1007/s10237-005-0070-2)

Milani, A. S., Nemes, J. A., Abeyaratne, R. C. & Holzapfel, G. A. 2007 A method for the approximation of non-uniform fiber misalignment in textile composites using picture frame test. *Composites Part A* **38**, 1493–1501. (doi:10.1016/j.compositesa.2007.01.008)

Mortier, P., Holzapfel, G. A., De Beule, M., Van Loo, D., Taeymans, Y., Segers, P., Verdonck, P. & Verhegghe, B. 2010 A novel simulation strategy for stent insertion and deployment in curved coronary bifurcations: comparison of three drug-eluting stents. *Ann. Biomed. Eng.* **38**, 88–99. (doi:10.1007/s10439-009-9836-5)

Murtada, S., Kroon, M. & Holzapfel, G. A. In press. A calcium-driven mechanochemical model for prediction of force generation in smooth muscle. *Biomech. Model. Mechanobiol.*

Murtada, S., Kroon, M. & Holzapfel, G. A. Submitted. Modeling the dispersion effects of contractile fibres in smooth muscles.

Nam, T. H. & Thinh, T. I. 2006 Large deformation analysis of inflated air-spring shell made of rubber-textile cord composite. *Struct. Eng. Mech.* **24**, 31–50.

Nguyen, T. D., Jones, R. E. & Boyce, B. L. 2008 A nonlinear anisotropic viscoelastic model for the tensile behavior of the corneal stroma. *J. Biomech. Eng.* **130**, 041020. (doi:10.1115/1.2947399)

Niroomandi, S., Alfaro, I., Cueto, E. & Chinesta, F. 2008 Real-time deformable models of non-linear tissues by model reduction techniques. *Comput. Methods Programs Biomed.* **91**, 223–231. (doi:10.1016/j.cmpb.2008.04.008)

Ogden, R. W. 1997 *Non-linear elastic deformations.* New York, NY: Dover.

Ogden, R. W. 2003 Nonlinear elasticity, anisotropy, material stability and residual stresses in soft tissue. In *Biomechanics of soft tissue in cardiovascular systems* (eds G. A. Holzapfel & R. W. Ogden), pp. 65–108. CISM Courses and Lectures no. 441. Vienna, Austria: Springer.

Ogden, R. W. 2009 Anisotropy and nonlinear elasticity in arterial wall mechanics. In *Biomechanical modelling at the molecular, cellular and tissue levels* (eds G. A. Holzapfel & R. W. Ogden), pp.179–258. CISM Courses and Lectures no. 508. Vienna, Wien, Austria: Springer.

Olsson, T. & Klarbring, A. 2008 Residual stresses in soft tissue as a consequence of growth and remodeling: application to an arterial geometry. *Eur. J. Mech. A Solids* **27**, 959–974. (doi:10.1016/j.euromechsol.2007.12.006)

Pandolfi, A. & Holzapfel, G. A. 2008 Three-dimensional modeling and computational analysis of the human cornea considering distributed collagen fibril orientations. *J. Biomech. Eng.* **130**, 061006.

Pandolfi, A. & Manganiello, F. 2006 A model for the human cornea. Constitutive formulation and numerical analysis. *Biomech. Model. Mechanobiol.* **5**, 237–246. (doi:10.1007/s10237-005-0014-x)

Peña, E., Calvo, B., Martínez, M. A. & Doblaré, M. 2008*a* On finite-strain damage of viscoelastic-fibred materials. Application to soft biological tissues. *Int. J. Numer. Meth. Eng.* **74**, 1198–1218.

Peña, E., Martínez, M. A., Calvo, B. & Doblaré, M. 2008*b* Application of the natural element method to finite deformation inelastic problems in isotropic and fiber-reinforced biological soft tissues. *Comput. Meth. Appl. Mech. Eng.* **197**, 1983–1996.

Pierce, D. M., Trobin, W., Trattnig, S., Bischof, H. & Holzapfel, G. A. 2009 A phenomenological approach toward patient-specific computational modeling of articular cartilage including collagen fiber tracking. *J. Biomech. Eng.* **131**, 091006. (doi:10.1115/1.3148471)

Prot, V. & Skallerud, B. 2009 Nonlinear solid finite element analysis of mitral valves with heterogeneous leaflet layers. *Comput. Mech.* **43**, 353–368. (doi:10.1007/s00466-008-0310-2)

Prot, V., Skallerud, B. & Holzapfel, G. A. 2007 Transversely isotropic membrane shells with application to mitral valve mechanics. Constitutive modelling and finite element implementation. *Int. J. Numer. Meth. Eng.* **71**, 987–1008. (doi:10.1002/nme.1983)

Prot, V., Skallerud, B., Sommer, G. & Holzapfel, G. A. 2010 On modelling and analysis of healthy and pathological human mitral valves: two case studies. *J. Mech. Behav. Biomed. Mat.* **3**, 167–177. (doi:10.1016/j.jmbbm.2009.05.004)

Rachev, A. & Hayashi, K. 1999 Theoretical study of the effects of vascular smooth muscle contraction on strain and stress distributions in arteries. *Ann. Biomed. Eng.* **27**, 459–468. (doi:10.1114/1.191)

Rissland, P., Alemu, Y., Einav, S., Ricotta, J. & Bluestein, D. 2009 Abdominal aortic aneurysm risk of rupture: patient-specific FSI simulations using anisotropic model. *J. Biomech. Eng.* **131**, 031001. (doi:10.1115/1.3005200)

Rodriguez, E. K., Hoger, A. & McCulloch, A. D. 1994 Stress-dependent finite growth in soft elastic tissues. *J. Biomech.* **27**, 455–467. (doi:10.1016/0021-9290(94)90021-3)

Rodríguez, J., Goicolea, J. M. & Gabaldón, F. 2007 A volumetric model for growth of arterial walls with arbitrary geometry and loads. *J. Biomech.* **40**, 961–971. (doi:10.1016/j.jbiomech.2006.05.002)

Rodríguez, J. F., Alastrue, V. & Doblaré, M. 2008*a* Finite element implementation of a stochastic three dimensional finite-strain damage model for fibrous soft tissue. *Comput. Meth. Appl. Mech. Eng.* **197**, 946–958. (doi:10.1016/j.cma.2007.09.017)

Rodríguez, J. F., Ruiz, C., Doblaré, M. & Holzapfel, G. A. 2008*b* Mechanical stresses in abdominal aortic aneurysms: influence of diameter, asymmetry and material anisotropy. *J. Biomech. Eng.* **130**, 021023–1–10.

Rodríguez, J. F., Martufi, G., Doblaré, M. & Finol, E. A. 2009 The effect of material model formulation in the stress analysis of abdominal aortic aneurysms. *Ann. Biomed. Eng.* **37**, 2218–2221. (doi:10.1007/s10439-009-9767-1)

Schulze-Bauer, C. A. J. & Holzapfel, G. A. 2003 Determination of constitutive equations for human arteries from clinical data. *J. Biomech.* **36**, 165–169. (doi:10.1016/S0021-9290(02)00367-6)

Sommer, G., Gasser, T. C., Regitnig, P., Auer, M. & Holzapfel, G. A. 2008 Dissection of the human aortic media: an experimental study. *J. Biomech. Eng.* **130**, 021007–1–12.

Sommer, G., Regitnig, P., Költringer, L. & Holzapfel, G. A. 2010 Biaxial mechanical properties of intact and layer-dissected human carotid arteries at physiological and supraphysiological loadings. *Am. J. Physiol. Heart Circ. Physiol.* **298**, H898–H912. (doi:10.1152/ajpheart.00378.2009)

Speirs, D. C., de Souza Neto, E. A. & Peric, C. 2008 An approach to the mechanical constitutive modelling of arterial tissue based on homogenization and optimization. *J. Biomech.* **41**, 2673–2680. (doi:10.1016/j.jbiomech.2008.06.020)

Stålhand, J. 2009 Determination of human arterial wall parameters from clinical data. *Biomech. Model. Mechanobiol.* **8**, 141–148.

Stålhand, J., Klarbring, A. & Holzapfel, G. A. 2008 Smooth muscle contraction: mechanochemical formulation for homogeneous finite strains. *Prog. Biophys. Mol. Biol.* **96**, 465–481.

Tang, D., Yang, C., Kobayashi, S., Zheng, J., Woodard, P. K., Teng, Z., Billiar, K., Bach, R. & Ku, D. N. 2009 3D MRI-based anisotropic FSI models with cyclic bending for human coronary atherosclerotic plaque mechanical analysis. *J. Biomech. Eng.* **131**, 061010. (doi:10.1115/1.3127253)

Taylor, C. A. & Humphrey, J. D. 2009 Open problems in computational vascular biomechanics: hemodynamics and arterial wall mechanics. *Comput. Meth. Appl. Mech. Eng.* **198**, 3514–3523. (doi:10.1016/j.cma.2009.02.004)

Valentín, A. & Humphrey, J. D. 2009 Parameter sensitivity study of a constrained mixture model of arterial growth and remodeling. *J. Biomech. Eng.* **131**, 101006. (doi:10.1115/1.3192144)

Vande Geest, J. P., Sacks, M. S. & Vorp, D. A. 2004 Age dependency of the biaxial biomechanical behavior of human abdominal aorta. *J. Biomech. Eng.* **126**, 815–822. (doi:10.1115/1.1824121)

Vena, P., Gastaldi, D., Socci, L. & Pennati, G. 2008 An anisotropic model for tissue growth and remodeling during early development of cerebral aneurysms. *Comp. Mater. Sci.* **43**, 565–577. (doi:10.1016/j.commatsci.2007.12.023)

Volokh, K. Y. 2007 Hyperelasticity with softening for modeling materials failure. *J. Mech. Phys. Solids* **55**, 2237–2264. (doi:10.1016/j.jmps.2007.02.012)

Volokh, K. Y. 2008 Prediction of arterial failure based on a microstructural bi-layer fiber–matrix model with softening. *J. Biomech.* **41**, 447–453. (doi:10.1016/j.jbiomech.2007.08.001)

Volokh, K. Y. & Vorp, D. A. 2008 A model of growth and rupture of abdominal aortic aneurysm. *J. Biomech.* **41**, 1015–1021. (doi:10.1016/j.jbiomech.2007.12.014)

Vossoughi, J., Vaishnav, R. N. & Patel, D. J. 1980 Compressibility of the myocardial tissue. In *Advances in bioengineering* (ed. V. C. Mow), pp. 45–48. ASME BED. New York, NY: American Society of Mechanical Engineers.

Watton, P. N. & Hill, N. A. 2009 Evolving mechanical properties of a model of abdominal aortic aneurysm. *Biomech. Model. Mechanobiol.* **8**, 25–42. (doi:10.1007/s10237-007-0115-9)

Watton, P. N., Hill, N. A. & Heil, M. 2004 A mathematical model for the growth of the abdominal aortic aneurysm. *Biomech. Model. Mechanobiol.* **3**, 98–113. (doi:10.1007/s10237-004-0052-9)

Weisstein, E. W. 2010 Erfi. MathWorld—a Wolfram Web Resource. See http://mathworld.wolfram.com/Erfi.html.

Wicker, B. K., Hutchens, H. P., Wu, Q., Yeh, A. T. & Humphrey, J. D. 2008 Normal basilar artery structure and biaxial mechanical behavior. *Comput. Methods Biomech. Biomed. Eng.* **11**, 539–551. (doi:10.1080/10255840801949793)

Wiechert, L., Metzke, R. & Wall, W. A. 2009 Modeling the mechanical behavior of lung tissue at the microlevel. *J. Engr. Mech.* **135**, 434–438. (doi:10.1061/(ASCE)0733-9399(2009)135:5(434))

Yang, J., Clark Jr, J. W., Bryan, R. M. & Robertson, C. S. 2003*a* The myogenic response in isolated rat cerebrovascular arteries: smooth muscle cell model. *Med. Eng. Phys.* **25**, 691–709. (doi:10.1016/S1350-4533(03)00100-0)

Yang, J., Clark Jr, J. W., Bryan, R. M. & Robertson, C. S. 2003*b* The myogenic response in isolated rat cerebrovascular arteries: vessel model. *Med. Eng. Phys.* **25**, 711–717. (doi:10.1016/S1350-4533(03)00101-2)

Yang, W., Fung, T. C., Chian, K. S. & Chong, C. K. 2006 Directional, regional, and layer variations of mechanical properties of esophageal tissue and its interpretation using a structure-based constitutive model. *J. Biomech. Eng.* **128**, 409–418. (doi:10.1115/1.2187033)

Yang, C., Bach, R. G., Zheng, J., Naqa, I. E., Woodard, P. K., Teng, Z., Billiar, K. & Tang, D. 2009 *In vivo* IVUS-based 3-D fluid–structure interaction models with cyclic bending and anisotropic vessel properties for human atherosclerotic coronary plaque mechanical analysis. *IEEE T. Biomed. Eng.* **56**, 2420–2428. (doi:10.1109/TBME.2009.2025658)

Zeinali-Davarani, S., Choi, J. & Baek, S. 2009 On parameter estimation for biaxial mechanical behavior of arteries. *J. Biomech.* **42**, 524–530. (doi:10.1016/j.jbiomech.2008.11.022)

Zulliger, M. A., Fridez, P., Hayashi, K. & Stergiopulos, N. 2004*a* A strain energy function for arteries accounting for wall composition and structure. *J. Biomech.* **37**, 989–1000. (doi:10.1016/j.jbiomech.2003.11.026)

Zulliger, M. A., Rachev, A. & Stergiopulos, N. 2004*b* A constitutive formulation of arterial mechanics including vascular smooth muscle tone. *Am. J. Physiol. Heart Circ. Physiol.* **287**, H1335–H1343. (doi:10.1152/ajpheart.00094.2004)